Available online at www.sciencedirect.com

ScienceDirect

Nuclear Physics B 931 (2018) 506–536

NUCLEAR PHYSICS B

www.elsevier.com/locate/nuclphysb

Thermalization of holographic Wilson loops in spacetimes with spatial anisotropy

D.S. Ageev [a,*], I.Ya. Aref'eva [a], A.A. Golubtsova [b,c], E. Gourgoulhon [d]

[a] *Steklov Mathematical Institute, Russian Academy of Sciences, Gubkina str. 8, 119991, Moscow, Russia*
[b] *Bogoliubov Laboratory of Theoretical Physics, JINR, 141980 Dubna, Moscow region, Russia*
[c] *Dubna State University, Universitetskaya str. 19, Dubna, 141980, Russia*
[d] *Laboratoire Univers et Théories, Observatoire de Paris, Université PSL, CNRS, Université Paris Diderot, 5 place Jules Janssen, 92190 Meudon, France*

Received 29 August 2017; received in revised form 16 April 2018; accepted 25 April 2018
Available online 27 April 2018
Editor: Leonardo Rastelli

Abstract

In this paper, we study behavior of Wilson loops in the boost-invariant nonequilibrium anisotropic quark–gluon plasma produced in heavy-ion collisions within the holographic approach. We describe the thermalization studying the evolution of the Vaidya metric in the boost-invariant and spatially anisotropic background. To probe the system during this process we calculate rectangular Wilson loops oriented in different spatial directions. We find that anisotropic effects are more visible for the Wilson loops lying in the transversal plane unlike the Wilson loops with partially longitudinal orientation. In particular, we observe that the Wilson loops can thermalizes first unlike to the order of the isotropic model. We see that Wilson loops on transversal contours have the shortest thermalization time. We also calculate the string tension and the pseudopotential at different temperatures for the static quark–gluon plasma. We show that the pseudopotential related to the configuration on the transversal plane has the screened Cornell form. We also show that the jet-quenching parameter related with the average of the light-like Wilson loop exhibits the dependence on orientations.

* Corresponding author.
E-mail addresses: ageev@mi.ras.ru (D.S. Ageev), arefeva@mi.ras.ru (I.Ya. Aref'eva), golubtsova@theor.jinr.ru (A.A. Golubtsova), eric.gourgoulhon@obspm.fr (E. Gourgoulhon).

https://doi.org/10.1016/j.nuclphysb.2018.04.016

1. Introduction

Wilson loops are known to play a key role as fundamental probes of gauge theories, in particular QCD. Owing to Wilson loops one can define many important quantities, for instance, we can derive the potential of a quark–antiquark interaction from the expectation value of the space–time rectangular Wilson loop. In the lattice QCD the Wilson loops are the prime observables and their expectation values are defined non-perturbatively [1]. One can also determine expectation values of Wilson loops in the framework of perturbative QCD after suitable renormalization [2].

At the same time, expectation values of Wilson loops are used to characterize properties of the quark–gluon plasma produced in heavy ion collisions (HIC). With the help of Wilson loops one can perform the analysis of radiative parton energy loss, quarkonium suppression, jet quenching, etc. [3].

In this paper, we investigate the behavior of Wilson loops in the nonequilibrium spatially anisotropic quark–gluon plasma (QGP) produced in heavy-ion collisions in the framework of the holographic correspondence. It is widely appreciated that the holography, or the gauge/gravity duality, provides a powerful tool for studying dynamics of the strong coupling system, in particular, the QGP formed in heavy-ion collisions [3–5]. Main idea of this approach is using natural prescriptions of the generalized AdS/CFT correspondence to recover non-perturbative QCD phenomena, particularly, non-perturbative vacuum phenomena, finite temperature, high-dense and non-zero chemical potential phenomena. In this strategy, fitting parameters are ones specifying the form of the 5-dimensional metric. The 5-dimensional background is supposed to be a solution of Einstein equations with a suitable matter content, not necessary related with string theory.

According to the holographic approach, creation of the quark–gluon plasma in HIC can be represented here as a collision of shock waves in the 5-dimensional bulk, in which a black hole is formed [6–15]. After the collision the shocks slowly decay, leaving the plasma described by hydrodynamics. The formation of the black hole can be also described by an infalling shell [16] propagating in the 5-dimensional bulk. A gravitational collapse of the thin shell to the black hole provides also a gravitational dual description of a more general class of thermalization processes [17–19]. Note, that the holographic approach is convenient to incorporate anisotropic properties of the QGP created in heavy-ion collisions [20,21].

The holographic approach has been widely used to study Wilson loops in different settings. Expectation values of Wilson loops within the gauge/gravity duality have been calculated for the strongly coupled $\mathcal{N} = 4$ super Yang–Mills theory [22–25]. The string dual description of the real QCD is unknown in spite of a lot of performed effort to find it [26–28]. However, suitable "bottom-up" holographic QCD models matching with experimental and lattice results have been proposed in [29–37]. Various physical quantities, in particular, expectation values of Wilson loops, have been calculated holographically. Wilson loops in static anisotropic backgrounds, static non-relativistic background, Lifshitz backgrounds and backgrounds with hyperscaling violation have been examined in [21], [38–44] and references therein. As it is known following the holographic dictionary, gravity duals of light-like Wilson loops can be used for calculation of the jet quenching parameter [45,46] controlling the description of medium-induced energy loss for partons in QCD. Holographic evaluation of the jet-quenching parameter for anisotropic QGP was considered in [41,42,21].

The special feature of this paper is that we consider spatially anisotropic backgrounds, which have also boost invariance

$$ds^2 = \frac{R^2}{z^2}\left(-dt^2 + dx^2 + (\frac{aR}{z})^{2/\nu-2}(dy_1^2 + dy_2^2) + dz^2\right). \tag{1}$$

These backgrounds are characterized by the scale parameter R and anisotropic parameters a and ν.

This spacetime is in accordance with the geometry of HIC, where one has a selected direction – the axis of ions collisions. As has been shown before [47], to fit the experimental form of the dependence of total multiplicity on energy, obtained at LHC, one can assume that the holographic model has boost invariance and a spatial anisotropy controlled by the so-called critical exponent. More precisely, it has been shown in [47] that the critical exponent should be taken $\nu = 4.45$. The metrics of the form (1) are dual to models with so called Lifshitz-like fixed points [48, 49]. These metrics are also occurs as the IR limit for the anisotropic background suggested for studies of QGP in [50]. It's also worth to be noted that the anizotropic background (1) differs from the Lifshitz metrics [51] by the anisotropic scaling of spatial coordinates. The Vaidya shell in the background (1) has been found in [53] and used to estimate the thermalization time of the 2-point correlators and the holographic entanglement entropy in HIC [52,53]. The holographic model with the shell in (1) was used to explore the behavior of the quark–antiquark potential in [54] with the method developed previously for in the AdS-Vaidya background [55].

As already mentioned, the information about processes during HIC can be read off from the expectation values of Wilson loops. Thus, it is natural to study the behavior of Wilson loops during the HIC within the same holographic model we used to fit the energy dependence of total multiplicity. In particular, it is reasonable to investigate thermalization of Wilson loops and their behavior in the end of the thermalization process. By thermalization of Wilson loop we mean the thermalization of its expectation value.

In the present work we calculate holographically Wilson loops in the backgrounds (1) with the Vaidya shell and black brane. We consider spatial and light-like configurations, which represent rectangles with two infinitely long sides and two sides of finite lengths. By virtue of the metric (1) possessing a spatial anisotropy, the expectation values of Wilson loops depend on the orientation of the corresponding configuration. Further, we will study potentials and its evolution during the thermalization process. We show that the order of thermalization in our background is the following: first thermalizes two-point correlator, then Wilson loops and the last thermalization occurs for the entanglement entropy. Our anisotropy reduces the thermalization time for non-local observables as compared to the isotropic case. We also find an analytical representation for the holographic light-like Wilson loops in the background (1) and derive the jet quenching parameter.

The paper is organized as the following. In Sec. 2 we briefly remind the holographic description of Wilson loops, gravitational backgrounds and the notations. In Sec. 3 we analyze the static Wilson loops as well as calculate pseudopotentials, string tensions for different orientations of Wilson loop and the jet quenching parameter. In Sec. 4 we study the nonequilibrium dynamics of the same oriented Wilson loops and present the results. In Sec. 5 the thermalization time of Wilson loops is estimated and we compare it with the thermalization times of the entanglement entropy and two-point correlation functions. We conclude with a discussion of our results and further directions.

2. Set up

2.1. Wilson loops

In this work we consider rectangular Wilson loops. As already noticed, Wilson loops contain the information about the force between quarks. Following the holographic approach [22,23] the expectation value of the Wilson loop in the fundamental representation calculated on the gravity side reads as:

$$W[C] = \langle \mathrm{Tr}_F\, e^{i \oint_C dx_\mu A_\mu} \rangle = e^{-S_{string}[C]}, \tag{2}$$

where C in a contour on the boundary. More precisely, we mean that the contour is at the "regularized boundary" $z = z_0$. On the gauge side we suppose to deal with the Wilson loop in the anisotropic gauge theory, i.e. theory on the 4-dimensional flat anisotropic background,

$$ds_4^2 = -dt^2 + dx^2 + (\frac{aR}{z_0})^{2/\nu-2}(dy_1^2 + dy_2^2). \tag{3}$$

The regularized version of this theory corresponds to the gauge theory on the anisotropic lattice [56], where spacing in the longitudinal and transversal directions, $a_\parallel$ and $a_\perp$, are different so that $a_\parallel/a_\perp = (aR/z_0)^{1-1/\nu}$. One can develop renormalizations in this theory and also the renormalization of the Wilson loops in the analogy with the isotropic theory. F means the fundamental representation (we will omit this symbol in what follows), S_{string} is the minimal action of the string hanging from the contour C in the bulk. The Nambu–Goto action can be represented as

$$S_{string} = \frac{1}{2\pi\alpha'} \int d\sigma^1 d\sigma^2 \sqrt{-\det(h_{\alpha\beta})}, \tag{4}$$

with $h_{\alpha\beta} = g_{MN}\partial_\alpha X^M \partial_\beta X^N$. In (4) σ^1, σ^2 parametrize the worldsheet, g_{MN} is the background metric, $M, N = 1, \ldots, 5$ and $X^M = X^M(\sigma^1, \sigma^2)$ specify the string worldsheet.

The pseudopotential of the interquark interaction can be extracted from the rectangular spatial Wilson loop of size[1] $\ell \times L$, for large L

$$W(\ell, L) = \langle \mathrm{Tr}\, e^{i \oint_{\ell\times L} dx_\mu A_\mu} \rangle = e^{-\mathcal{V}(\ell)L}, \tag{5}$$

and its defines the so called pseudopotential $\mathcal{V}$. We note, that for large L the behavior of $W(\ell, L)$ is different from the behavior of the time-like one. Then the pseudopotential can be straightforwardly extracted from the string action (4) as follows

$$\mathcal{V}(\ell) = \frac{S_{string}}{L}. \tag{6}$$

As it is known from the QCD lattice calculations the spatial Wilson loops obey the area law at all temperature, i.e. the spatial string tension σ_s is given by

$$\sigma_s = \lim_{\ell\to\infty} \frac{\mathcal{V}(\ell)}{\ell}. \tag{7}$$

The quantity σ_s differs from the usual string tension which is defined from time-like Wilson-loops. By virtue to the non-Abelian Stokes formula equal time spatial Wilson loops [57] are related with the spatial components of the energy–momentum tensor and by this reason σ_s is also called the magnetic string tension. Spatial Wilson loops have been studied on the lattice [58,59], analytically [60], and also within the gauge/gravity duality [62,61].

[1] Note that we take $\ell < L$ for real calculations, where ℓ is large, but not infinite.

2.2. The boost invariant anisotropic metrics

We will study spatial Wilson loops in gravity backgrounds with spatial anisotropy, given by (1), where the critical exponent ν controls the deviation from isotropic case. In [53] we have called this metric as an Lifshitz-like metrics. In this paper to avoid a misleading with the Lifshitz metrics we mainly call the metric (1) as the boost invariant spatial anisotropic metric. Note, that in (1) we used the standard dimensional coordinates. In what follows we take $R^2 = 2\pi\alpha'$, $a = 1$ and use the dimensionless coordinates $\tilde{t} = t/(2\pi\alpha')^{1/2}$, $\tilde{z} = z/(2\pi\alpha')^{1/2}$ etc., and we remove tilde on the top of coordinates. So, the metric take the form

$$ds^2 = 2\pi\alpha'\left(\frac{-dt^2+dx^2}{z^2} + \frac{dy_1^2+dy_2^2}{z^{2/\nu}} + \frac{dz^2}{z^2}\right). \tag{8}$$

One can see that the background (8) with $\nu = 1$ comes to be the 5-dimensional AdS space-time. As already mentioned, the choice of this metric is motivated by the fact that holographic estimations of the total multiplicity performed in this background reproduce the experimental dependence of the multiplicity on the energy [47].

The non-zero temperature generalization of (1) was constructed in [53][2]:

$$ds^2 = 2\pi\alpha'\left(\frac{-f(z)dt^2+dx^2}{z^2} + \frac{dy_1^2+dy_2^2}{z^{2/\nu}} + \frac{dz^2}{z^2 f(z)}\right), \tag{9}$$

with the blackening function

$$f = 1 - mz^{2+2/\nu}. \tag{10}$$

For $\nu = 1$ the background (9) with (10) represents the metric of the AdS black brane.

This background (9)–(10) describes holographically the anisotropic media on the boundary with the temperature corresponding to the Hawking temperature of the black brane:

$$T = \frac{1}{\pi}\frac{(\nu+1)}{2\nu}\, m^{\frac{\nu}{2\nu+2}}. \tag{11}$$

To study the thermalization process, corresponding to the black brane formation in the dual language, we will use the Vaidya generalization of solution (1)
[53]:

$$ds^2 = 2\pi\alpha'\left(-\frac{f(v,z)dv^2+2dvdz-dx^2}{z^2} + \frac{dy_1^2+dy_2^2}{z^{2/\nu}}\right) \tag{12}$$

with

$$f = 1 - m(v)z^{2+2/\nu}. \tag{13}$$

The metric (12) has been written in ingoing Eddington–Finkelstein coordinates (v, r). The function $m(v)$ in (13) defines the thickness of the shell smoothly interpolating between the zero-temperature (1) at $v = -\infty$ and black brane backgrounds (9) at $v = \infty$.

[2] The computations have been checked with SageManifolds, which is an extension of the free computer algebra system SageMath. The corresponding worksheets are publicly available at the following links:
https://cloud.sagemath.com/3edbca82-97d6-41b3-9b6f-d83ea06fc1e9/raw/Lifshitz_black_brane.html,
https://cloud.sagemath.com/3edbca82-97d6-41b3-9b6f-d83ea06fc1e9/raw/Vaidya-Lifshitz.html.

We choose the following form for the function f

$$f(z,v) = 1 - \frac{m}{2}\left(1 + \tanh\frac{v}{\alpha}\right) z^{\frac{2}{\nu}+2}, \tag{14}$$

where α is a parameter. For the calculations in this paper we keep $\alpha = 0.2$.

3. Spatial Wilson loops in a time-independent background

In this work we consider rectangular Wilson loops in the static background (9) located in the spatial planes xy_1 (or xy_2) and y_1y_2. One can delineate the following possible configurations:

- a rectangular loop in the xy_1 (or xy_2) plane with a short side of the length ℓ_x in the longitudinal x direction and a long side of the length L_{y_1} along the transversal y_1 direction, so that

$$x \in [0, \ell_x], \quad y_1 \in [0, L_{y_1}], \quad \ell_x < L_{y_1}; \tag{15}$$

- a rectangular loop in the xy_1 plane with a short side of the length ℓ_{y_1} in the transversal y_1 direction and a long side of the length L_x along the longitudinal x direction,

$$x \in [0, L_x], \quad y_1 \in [0, \ell_{y_1}], \quad \ell_{y_1} < L_x; \tag{16}$$

- a rectangular loop in the transversal y_1y_2 plane with a short side of the length ℓ_{y_1} in one of transversal directions (say y_1) and a long side of the length L_{y_2} along the other transversal direction y_2, namely

$$y_1 \in [0, \ell_{y_1}], \quad y_1 \in [0, L_{y_2}], \quad \ell_{y_1} < L_{y_2}. \tag{17}$$

In this section we perform all calculations in the static spacetime (9) with (10) (using Eddington–Finkelstein coordinates).

3.1. Wilson loops on the xy_1-plane

3.1.1. Rectangular strip infinite along the y_1-direction

We start from the rectangular Wilson loop in the xy_1-plane assuming that the large extent is oriented in the y_1-direction (see (15)). We parametrize the world-sheet of the string in the following way $\sigma^1 = x, \quad \sigma^2 = y_1$, assuming $v = v(x)$, $z = z(x)$ and boundary conditions: $z(\pm\ell_x/2) = 0, z(0) = z_*, v(0) = v_*, z'(0) = 0, v'(0) = 0$.

Taking into account (4) and (12) with the stationary f given by (10), the Nambu–Goto action can be presented as

$$S_{x,y_{1(\infty)}} = \int dy_1 dx \frac{1}{z^{1/\nu}} \sqrt{\left(\frac{1}{z^2} - \frac{1}{z^2} f v'^2 - \frac{2}{z^2} v' z'\right)}, \tag{18}$$

where it is supposed $' \equiv \frac{d}{dx}$. The subscript $x, y_{1(\infty)}$ in the LHS of (18) indicates the orientation of the loop contour.

The action (18) on the time-independent string configurations after division on the length of the Wilson loop in the y_1-direction can be rewritten in the form

$$\frac{S_{x,y_{1(\infty)}}}{L_{y_1}} = \int \frac{dx}{z^{1+1/\nu}\sqrt{f}} \sqrt{f(z) + z'^2}. \tag{19}$$

The RHS of (19) defines a dynamical system that has the first integral

$$J = \frac{1}{z^{1+1/\nu}} \frac{\sqrt{f(z)}}{\sqrt{f(z) + z'^2}}. \tag{20}$$

Note, that the same is true for the action in the form (18). Indeed, it defines the dynamical system with two degrees of freedom, $z = z(x)$ and $v = v(x)$, that for the stationary case has two integral of motions and excluding v due to the conservation law one comes back to (20).

Since we have the symmetric boundary conditions, the top of the configuration $z = z(x)$ is at $x = 0$, i.e. $z_* = z(0)$ and $z'(0) = 0$, and z_* is related with the first integral,

$$\frac{1}{z^{1+1/\nu}} \frac{\sqrt{f(z)}}{\sqrt{f(z) + z'^2}} = \frac{1}{z_*^{1+1/\nu}} \tag{21}$$

Equation (21) and the boundary condition $z(\pm \ell_x/2) = 0$ give us the relation between the top point z_* and the length

$$\ell_x = 2 \int_{z_0}^{z_*} \frac{dz}{\sqrt{f(z)\left(\left(\frac{z_*}{z}\right)^{2+2/\nu} - 1\right)}}. \tag{22}$$

So the Nambu–Goto action (18) can be rewritten in the form

$$\frac{S_{x,y_{1(\infty)}}}{L_{y_1}} = 2 \int_{z_0}^{z_*} \frac{dz}{z^{1+1/\nu}\sqrt{f(z)}} \frac{1}{\sqrt{1 - \left(\frac{z}{z_*}\right)^{2+2/\nu}}}. \tag{23}$$

Here we use the regularized boundary conditions $z(\pm \ell_x/2) = z_0$. The action (23) has a divergent when $z_0 \to 0$ and one can present it in the form

$$\frac{S_{x,y_{1(\infty)}}}{2L_{y_1}} = \frac{1}{z_*^{1/\nu}} \int_{z_0/z_*}^{1} \frac{dw}{w^{1+1/\nu}} \left[\frac{1}{\sqrt{f(z_* w)\left(1 - w^{2+2/\nu}\right)}} - 1\right] + \frac{1}{z_*^{1/\nu}} \int_{z_0/z_*}^{1} \frac{dw}{w^{1+1/\nu}}. \tag{24}$$

Subtracting the divergent part $\frac{\nu}{z_0^{1/\nu}}$ one gets the renormalized Nambu–Goto action

$$\frac{S_{x,y_{1(\infty)},ren}}{2L_{y_1}} = \frac{1}{z_*^{1/\nu}} \int_{0}^{1} \frac{dw}{w^{1+1/\nu}} \left[\frac{1}{\sqrt{f(z_* w)\left(1 - w^{2+2/\nu}\right)}} - 1\right] - \frac{\nu}{z_*^{1/\nu}}. \tag{25}$$

The length (22) between the ends of the string admits the removing of regularization $z_0 \to 0$ without renormalization

$$\ell_x = 2 z_* \int_{0}^{1} \frac{w^{1+1/\nu}\, dw}{\sqrt{f(z_* w)(1 - w^{2+2/\nu})}}. \tag{26}$$

Then pseudopotential $\mathcal{V}_{x,y_{1(\infty)}}$ is given by:

$$\mathcal{V}_{x,y_{1(\infty)}} = \frac{S_{x,y_{1(\infty)},ren}}{L_{y_1}}. \tag{27}$$

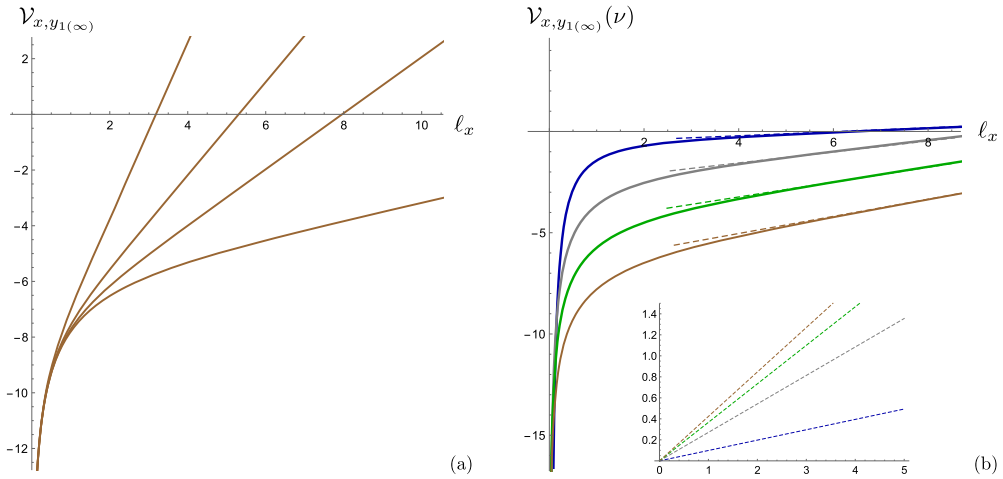

Fig. 1. a) The pseudopotential $\mathcal{V}_{x,y_{1(\infty)}}$ corresponding to the action $S_{x,y_{1(\infty)}}$ (25) as a function of ℓ_x (26) for $\nu = 4$. We take the temperature $T = 0.08, 0.2, 0.3, 0.5$ (from down to top). b) The behavior of the pseudopotential corresponding to (25) for $\nu = 1, 2, 3, 4$ (blue, gray, green and brown, respectively) at $T = 0.1$. The dashed lines show the asymptotics at large ℓ_x given be (34) with (35). The inset plot zooms the slops of dashed lines. (For interpretation of the colors in the figure(s), the reader is referred to the web version of this article.)

In Fig. 1 we present the dependence of the pseudopotential $\mathcal{V}_{x,y_{1(\infty)}}$ (27) on the length (26). We see that for small ℓ_x the pseudopotential has the Coulomb part deformed by the critical exponent, thus

$$\mathcal{V}_{x,y_{1(\infty)}}(\ell_x,\nu) \underset{\ell_x\sim 0}{\sim} -\frac{\mathcal{C}_1(\nu)}{\ell_x^{1/\nu}}, \tag{28}$$

where $\mathcal{C}_1$ is some constant dependent on ν. Putting $m = 0$ in (25) and (26), we get the leading term (28), while taking corrections on m one has for $\nu = 4$

$$\mathcal{V}_{x,y_{1(\infty)}}(\ell_x,4) = -\frac{7.80}{\ell_x^{1/4}}\left(1 - 0.012\, m\, \ell_x^{5/2} + \mathcal{O}\left(m^2\,\ell_x^5\right)\right). \tag{29}$$

The asymptotics for arbitrary ν are presented in Appendix A. One should note that for small enough ℓ_x the behavior of $\mathcal{V}_{x,y_{1(\infty)}}$ extracted from (25) for all ν has a form of the deformed Coulomb law with the power equal to $1/\nu$ reproducing the Coulomb behavior of the pseudopotential in the case $\nu = 1$ (the AdS case).

For large distances ℓ_x the pseudopotential $\mathcal{V}_{x,y_{1(\infty)}}$ behaves as a linearly increasing function

$$\mathcal{V}_{x,y_{1(\infty)}}(\ell_x,\nu) \underset{\ell_x\to\infty}{\sim} \sigma_{s,1}(\nu)\,\ell_x. \tag{30}$$

To see this behavior let us note that to get the large ℓ_x we have to take z_* near z_h, or $z_*/z_h = w_0 \to 1$, and in this case the denominator in the integrands in the RHS of (26) and (25) behaves as

$$\sqrt{f(z_* w)(1 - w^{2+2/\nu})} \approx \frac{2(\nu+1)}{\nu}(1-w), \tag{31}$$

and we get the log-behavior for ℓ_x and $\mathcal{V}_{x,y_{1(\infty)}}$

$$\ell_x \sim -2\frac{\nu z_*}{(\nu+1)}\log(1-w_0), \tag{32}$$

$$\mathcal{V}_{x,y_{1(\infty)}} \sim -\frac{2}{z_*^{1/\nu}}\frac{\nu}{(\nu+1)}\log(1-w_0), \tag{33}$$

which lead us to the asymptotic

$$\mathcal{V}_{x,y_{1(\infty)}} \underset{\ell_x\to\infty}{\sim} \sigma_{s,1}(\nu)\,\ell_x, \tag{34}$$

where

$$\sigma_{s,1}(\nu) = 1/z_h^{1+1/\nu} = \left(\frac{2\pi T}{1+1/\nu}\right)^{1+1/\nu}. \tag{35}$$

From Fig. 1.b we see that the asymptotics of a $\mathcal{V}_{x,y_{1(\infty)}}$ at large ℓ_x is linear with the slope given by formula (35). The formula (35) exhibits the dependence on ν shown in the zoomed inset of Fig. 1.b.

The string tension (35) can be also seen by dimensional analysis keeping the anisotropic parameter a in (1). Indeed, since we are working with metric (9) and we can assign a factor A to t, x and z and factor $A^{1/\nu}$ to y_1 and y_2. Since the action S is invariant under this rescaling we have that $\sigma_{1,s} \sim \frac{S}{\ell_x L_{y_1}} \sim A^{-(1+1/\nu)} \sim T^{1+1/\nu}$.

3.1.2. Rectangular strip infinite along the x-direction

Another possible configuration in the xy_1 plane is the rectangular Wilson loop whose contour is infinite along the x-direction and has a finite size along the y_1-direction (see (16)). We specify this type of the configuration by the subscript y_1, $x_{(\infty)}$. For the parameterization we take $v = v(y_1)$, $z = z(y_1)$ with boundary conditions $z(\pm\ell_{y_1}/2) = 0$. By virtue to this assumption the Nambu–Goto action (4) reads

$$S_{y_1,\,x_{(\infty)}} = \int \frac{dy_1 dx}{z}\sqrt{\left(\frac{1}{z^{2/\nu}} - \frac{1}{z^2}f(v')^2 - \frac{2}{z^2}v'z'\right)}, \tag{36}$$

where it is supposed $' \equiv \frac{d}{dy_1}$. Similar to the previous case this action can be rewritten as

$$\frac{S_{y_1,\,x_{(\infty)}}}{L_x} = \int \frac{dy_1}{z^2\sqrt{f}}\sqrt{f z^{2-2/\nu} + z'^2}, \tag{37}$$

and the first integral is related with the top point as

$$\frac{\sqrt{f(z)}z^{-2/\nu}}{\sqrt{f(z)z^{2-\frac{2}{\nu}} + z'^2}} = \frac{1}{z_*^{1+1/\nu}}. \tag{38}$$

Due to this relation we get the expression for the action

$$\frac{S_{y_1,\,x_{(\infty)}}}{L_x} = \frac{2}{z_*}\int\limits_{z_0/z_*}^{1}\frac{dw}{w^2}\frac{1}{\sqrt{f(z_*w)\left(1-w^{2+2/\nu}\right)}}, \tag{39}$$

and the length

$$\ell_{y_1} = 2z_*^{1/\nu}\int\limits_{z_0/z_*}^{1}\frac{w^{2/\nu}dw}{\sqrt{f(z_*w)\left(1-w^{2+2/\nu}\right)}}, \tag{40}$$

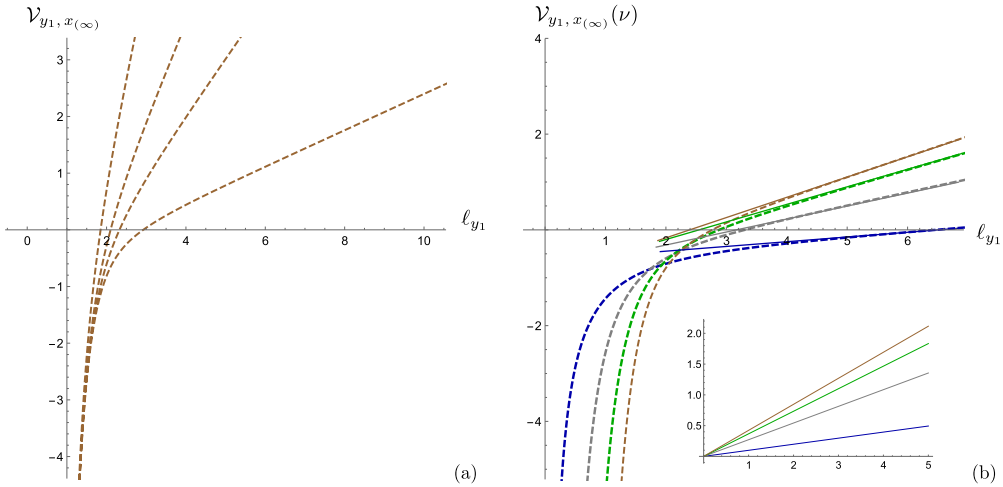

Fig. 2. a) The pseudopotential $\mathcal{V}_{y_1,x_{(\infty)}}$ extracted from action (41) as a function of ℓ_{y_1} for $\nu = 4$. We take $T = 0.08, 0.2, 0.3, 0.5$ from down to top. (q.6.1)b) The behavior of $\mathcal{V}_{y_1,x_{(\infty)}}$ for $\nu = 1, 2, 3, 4$ (blue, gray, green and brown, respectively) at $T = 0.1$. The solid thin lines show the asymptotic of $\mathcal{V}_{y_1,x_{(\infty)}}$ for large ℓ_y given by formula (45) for different ν. The inset plot zooms the slops of solid thin lines.

where z_0 is the regularization. Similar to the previous case one can remove regularization in (39) and in (40) after renormalization

$$\frac{S_{y_1,x_{(\infty)},ren}}{2L_x} = \frac{1}{z_*}\int_0^1 \frac{dw}{w^2}\left[\frac{1}{\sqrt{f(z_*w)\left(1-w^{2+2/\nu}\right)}} - 1\right] - \frac{1}{z_*}. \tag{41}$$

The pseudopotential $\mathcal{V}_{y_1,x_{(\infty)}}$ is related to (41) as

$$\mathcal{V}_{y_1,x_{(\infty)}} = \frac{S_{y_1,x_{(\infty)},ren}}{L_x}. \tag{42}$$

In Fig. 2 we show the dependence of the pseudopotential extracted from the action (41) on the length ℓ_{y_1} for different values of the temperature and the dynamical exponent. Now the pseudopotential has a power-law dependence on ν for small ℓ_{y_1}, so that

$$\mathcal{V}_{y_1,x_{(\infty)}} \underset{\ell_{y_1}\to 0}{\sim} -\frac{\mathcal{C}_2(\nu)}{\ell_{y_1}^{\nu}}, \tag{43}$$

with some constant $\mathcal{C}_2$ dependent on ν. One gets asymptotics (43) with $m = 0$ in (41) and (40), and taking corrections on m we obtain for $\nu = 4$

$$\mathcal{V}_{y_1,x_{(\infty)}} = -\frac{13.5}{\ell_{y_1}^4}\left(1 - 0.00031 m\ell_{y_1}^{10} + \mathcal{O}(m^2\ell_{y_1}^{20})\right). \tag{44}$$

However, for large distances the pseudopotential represents a linear function of ℓ_{y_1} again

$$\mathcal{V}_{y_1,x_{(\infty)}}(\ell_{y_1},\nu) \underset{\ell_{y_1}\to\infty}{\sim} \sigma_{s,2}(\nu)\,\ell_{y_1} \tag{45}$$

and using estimation, similar to (32) and (33) we get

$$\sigma_{s,2}(\nu) = \frac{1}{z_h^{1+1/\nu}} = (\frac{2\pi T}{1+1/\nu})^{1+1/\nu}, \tag{46}$$

that is also in agreement with the dimensional analysis.

From Fig. 2.b we also see that the dependence of $\mathcal{V}_{y_1,\, x_{(\infty)}}(\ell_{y_1}, \nu)$ on ℓ_{y_1} at large length is linear for all the dynamical exponent ν with the slops slightly deviating from the AdS case ($\nu = 1$).

3.2. *Wilson loop on the y_1y_2-plane*

Now we come to the spatial rectangular Wilson loop located on the y_1y_2-plane. Let us assume that the loop contour is infinite along the y_2-direction and has the finite extent of the length ℓ_{y_1} in the y_1-direction (see (17)). We specify this type of the orientation by the subscript $y_1,\ y_{2(\infty)}$, choosing only transversal coordinates for the parameterization of the worldsheet $\sigma^1 = y_1, \quad \sigma^2 = y_2$.

Taking into account, that $z(y_1)$ satisfying $z(\pm\ell_{y_1}/2) = 0$ one can represent the string action (4) in the following form

$$S_{y_1,\, y_{2(\infty)}} = \int \frac{dy_1 dy_2}{z^{\frac{1}{\nu}}} \sqrt{\frac{1}{z^{\frac{2}{\nu}}} - \frac{f v'^2}{z^2} - \frac{2v'z'}{z^2}}, \tag{47}$$

where it is supposed $' \equiv \frac{d}{dy_1}$. Similar to the previous cases this action can be rewritten as

$$\frac{S_{y_1,\, y_{2(\infty)}}}{L_{y_2}} = \int \frac{dy}{z^{1+1/\nu}\sqrt{f}} \sqrt{f z^{2-2/\nu} + z'^2}, \tag{48}$$

and the first integral is related with z_* point as

$$\frac{\sqrt{f(z)} z^{1-\frac{3}{\nu}}}{\sqrt{f(z) z^{2-\frac{2}{\nu}} + z'^2}} = \frac{1}{z_*^{2/\nu}}. \tag{49}$$

Due to this relation we get the expression for the action

$$\frac{S_{y_1,\, y_{2(\infty)}}}{2L_{y_2}} = \int_{z_0}^{z_*} \frac{dz}{z^{1+1/\nu}} \frac{1}{\sqrt{f(z)\left(1 - \left(\frac{z}{z_*}\right)^{4/\nu}\right)}}, \tag{50}$$

and the length

$$\ell_{y_1} = \frac{2}{z_*^{2/\nu}} \int_{z_0}^{z_*} \frac{dz}{z^{1-3/\nu}\sqrt{f(z)\left(1 - \left(\frac{z}{z_*}\right)^{4/\nu}\right)}}, \tag{51}$$

where z_0 is the regularization. Similar to the previous case one can remove regularization in (51) directly and in (50) after renormalization. The renormalized action (50) in terms of the w-variable takes the form

$$\frac{S_{y_1,\, y_{2(\infty)},ren}}{2L_{y_2}} = \frac{1}{z_*^{1/\nu}} \int_{z_0/z_*}^{1} \frac{dw}{w^{1+1/\nu}} \Big[\frac{1}{\sqrt{f(z_* w)\left(1 - w^{4/\nu}\right)}} - 1 \Big] - \frac{\nu}{z_*^{1/\nu}}. \tag{52}$$

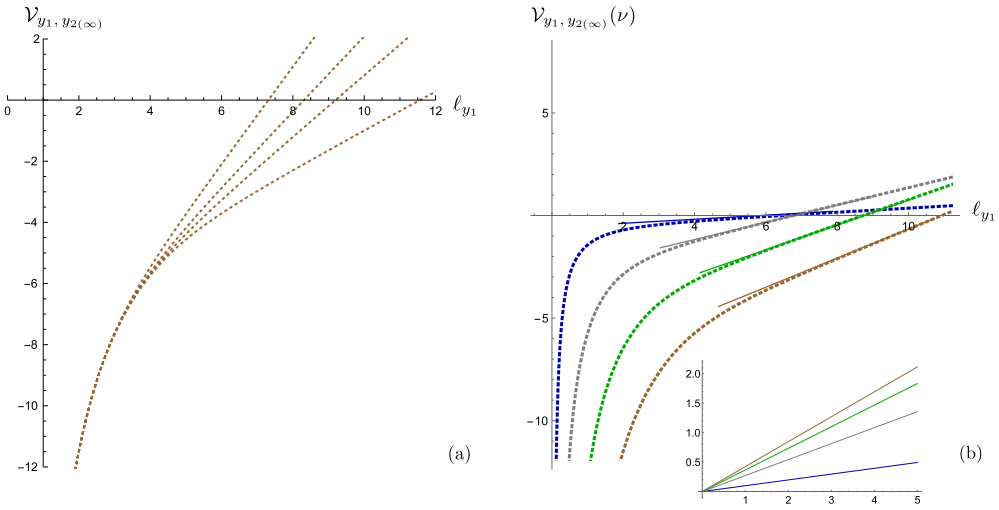

Fig. 3. a) The pseudopotential $\mathcal{V}_{y_1,\,y_{2(\infty)}}$ extracted from action (41) as a function of ℓ_{y_1} for $\nu = 4$. We take $T = 0.08, 0.2, 0.3, 0.5$ from down to top. The behavior of $\mathcal{V}_{y_1,\,x_{(\infty)}}$ corresponding to (41) for $\nu = 1, 2, 3, 4$ (from left to right, respectively) at $T = 0.1$. The solid lines show the asymptotics given by formula (56) with (57). The inset plot zooms the slops of solid thin lines.

The relation for the length is given by

$$\ell_{y_1} = 2z_*^{1/\nu} \int_0^1 \frac{dw}{w^{1-3/\nu}\sqrt{f(z_* w)\left(1-w^{4/\nu}\right)}}. \tag{53}$$

Finally, the pseudopotential $\mathcal{V}_{y_1,\,y_{2(\infty)}}$ extracted from (52) reads as:

$$\mathcal{V}_{y_1,\,y_{2(\infty)}} = \frac{S_{y_1,\,y_{2(\infty)}}}{L_{y_2}}. \tag{54}$$

In Fig. 3 we display the behavior of the pseudopotential (54) on the length (53).

It is easy to see that the behavior of $\mathcal{V}_{y_1,\,y_{2(\infty)}}$ in Fig. 3 is rather different from two previous cases. From Fig. 3 (b) we observe, that now the dependence on ν is driven by some constant $\mathcal{C}_3$ relying on ν. It should be noted that the pseudopotentials strongly deviate from the AdS case ($\nu = 1$) both in the UV and the IR regions of ℓ_{y_1}. Thus, one can write for small ℓ_{y_1}

$$\mathcal{V}_{y_1,\,y_{2(\infty)}}(\ell_{y_1},\nu) \underset{\ell_{y_1}\to 0}{\sim} -\frac{\mathcal{C}_3(\nu)}{\ell_{y_1}}, \tag{55}$$

where $\mathcal{C}_3$ is some constant dependent on ν. For $\nu = 4$ one can write down (55) with the corrections on m in the following form

$$\mathcal{V}_{y_1,\,y_{2(\infty)}}(\ell_{y_1}, 4) = -\frac{23.0}{\ell_{y_1}}\left(1 - 0.741\cdot 10^{-9} m\, l_{y_1}^{10} + \mathcal{O}\left(m^2 \ell_{y_1}^{20}\right)\right).$$

For large ℓ_{y_1} we have

$$\mathcal{V}_{y_1,\,y_{2(\infty)}}(\ell_{y_1},\nu) \underset{\ell_{y_1}\to\infty}{\sim} \sigma_{s,3}(\nu)\,\ell_{y_1}. \tag{56}$$

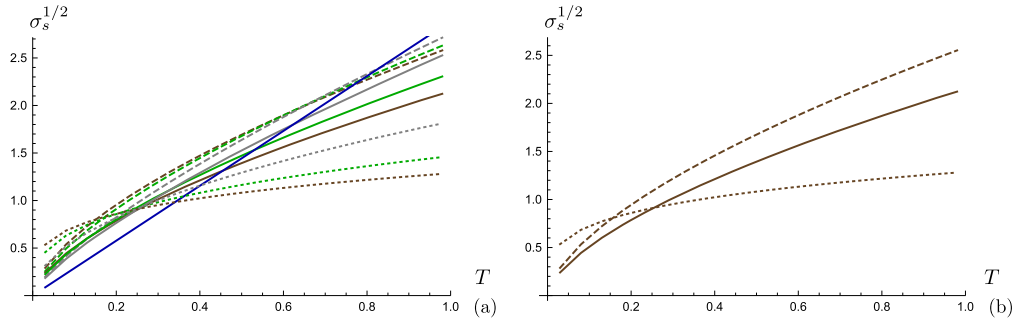

Fig. 4. The dependence of the spatial string tension $\sqrt{\sigma_s}$ on orientation and temperature. The solid lines corresponds to the rectangular Wilson loop with a short extent in the x-direction, while the dashed lines correspond to a short extent in the y-direction. The dotted lines correspond to the rectangular Wilson loop in the transversal y_1y_2-plane. (a) Blue line corresponds to $\nu = 1$, gray lines correspond to $\nu = 2$, green lines correspond to $\nu = 3$ and the brown ones correspond to $\nu = 4$. (b) The spatial string tension $\sqrt{\sigma_s}$ for different orientations for $\nu = 4$.

As in the previous cases the large ℓ_{y_1} behavior is provided by the pole near to $w \sim 1$ in (53) and we get, compare with (32) and (33),

$$\sigma_{s,3}(\nu) = \frac{1}{z_h^{2/\nu}} = \left(\frac{2\pi T}{1+1/\nu}\right)^{2/\nu}. \tag{57}$$

Looking at formulas (55)–(56) one can conclude that the pseudopotential corresponding to the configuration on the transversal plane reproduces the form of the Cornell potential.

3.3. Spatial string tension dependence on the orientation

It is interesting to analyze the behavior of the spatial string tension σ_s (7) for different orientations of the Wilson loop, i.e. the behavior of $\sigma_{s,i}, i = 1, 2, 3$ given by (30), (45) and (56). The temperature dependences of the spatial string tension in the confining background, which reproduces the Cornell potential [31], and the deconfining one have been studied in [62] and [63], respectively. In [64] the universal behavior of the spatial string tension for multiquark configurations was found. In the AdS/QCD model [31] the string tension dependence matching lattice data was found in [61].

In Fig. 4 (the left panel) we present the dependence of the spatial string tension $\sqrt{\sigma_s}$ as a function of T for all cases of the orientation and for $\nu = 1, 2, 3, 4$. We see, that for the configurations located on the xy_1-plane (partially longitudinal orientations shown by solid and dashed lines) the temperature dependence of the string tension for different ν are rather similar. The deviations of solid lines from dashed ones increase with increasing T. We also see that the string tension corresponding to the Wilson loop in the y_1y_2-plane (the totally transversal orientation shown by the dotted lines) differs from the behavior of the Wilson loop including the longitudinal direction, showing less dependence on the temperature with increasing ν. All these plots indicate that the structure of chromomagnetic fields in our holographic model has strong dependence on its orientation. In the right panel of Fig. 4 the spatial string tension $\sqrt{\sigma_s}$ for different orientations for $\nu = 4$ is presented.

We note that the behavior of magnetic Wilson loops in heavy ion collisions was worked out in [65,66] and is put in the context of the color glass condensate model. The universal behavior of a large magnetic Wilson loop was found to have a nontrivial power-law dependence on the loop

area. They have also argued that in contrast to usual Coulomb phase behavior, magnetic flux does not propagates uniformly in the transverse plane, but instead, it is concentrated in small domains. In our work the Coulomb phases of pseudopotentials are modified for orientations different from the transversal one.

3.4. The holographic light-like Wilson loops and jet-quenching

One of the important characterizations of heavy-ions collisions is the jet quenching. The jet-quenching parameter $\hat{q}$ introduced in [67] is related with the average of the light-like Wilson loop in the adjoint representation [68]

$$W_A(C) = e^{-\frac{1}{4\sqrt{2}}\hat{q}L_-\ell_{y_1}^2}, \tag{58}$$

where C is a rectangular contour with large extension L_- in a light-like direction and small extension ℓ_{y_1} in a transversal one. In the holographic approach $W_A(C)$ is equal to the classical string action S of a string worldsheet configuration stretched on the contour C on the boundary of the holographic background [45]

$$W_A(C) = e^{2iS}. \tag{59}$$

In this section we focus on holographic light-like Wilson loops in the black brane background (9). Choosing different light-like directions we obtain the dependence of the jet quenching parameter $\hat{q}$ on orientations.

Let us calculate the holographic light-like Wilson loop for the light-like coordinates related with the longitudinal direction, $x^{\pm} = \frac{t\pm x}{\sqrt{2}}$. The metric (9) in these light-cone coordinates takes the form

$$ds^2 = G_{--}(dx_+^2 + dx_-^2) + G_{-+}dx_-dx_+ + G_{y_1y_1}dy_1^2 + G_{y_2y_2}dy_2^2 + G_{zz}dz^2, \tag{60}$$

where

$$G_{--} = \frac{1-f(z)}{2z^2}, \quad G_{-+} = \frac{1+f(z)}{2z^2}, \quad G_{y_1y_1} = G_{y_2y_2} = \frac{1}{z^{2/\nu}},$$
$$G_{zz} = \frac{1}{z^2 f(z)}. \tag{61}$$

After introducing the parametrization for the string worldsheet by coordinates τ and σ such that

$$\tau = x^-, \quad \sigma = y_1, \quad z = z(y_1), \tag{62}$$

the string action takes the form

$$S = iL^- \int\limits_{-\ell_{y_1}/2}^{\ell_{y_1}/2} dy_1 \sqrt{G_{--}(G_{y_1y_1} + z'^2 G_{zz})}, \tag{63}$$

where i in front of the integral comes from the $\sqrt{-\det\gamma}$, since we deal with the Lorentz signature (here γ is the induced metric on the string). Note, that G_{--} is positive definite function when $z < z_h$. For small ℓ_{y_1} from this expression one gets [40]

$$\hat{q}^{-1} = \frac{1}{\sqrt{2}} \int\limits_0^{z_h} \frac{\sqrt{G_{zz}}}{\sqrt{G_{--}G_{y_1y_1}}} dz. \tag{64}$$

Evaluating the integral in (64) explicitly we get

$$\hat{q} = -\frac{2^{\frac{2}{\nu}+2}\nu^{\frac{\nu+2}{\nu}}\pi^{\frac{2}{\nu}-\frac{1}{2}}\Gamma\left(-\frac{\nu}{2\nu+2}\right)}{(\nu+1)^{\frac{2(\nu+1)}{\nu}}\Gamma\left(1+\frac{1}{2\nu+2}\right)}T^{\frac{\nu+2}{\nu}}. \tag{65}$$

For $\nu = 1$ formula (65) reproduces the T^3 dependence of the jet quenching parameter in the isotropic quark–gluon plasma [45], while in the case of $\nu > 1$ the dependence on the temperature of the jet quenching parameter is caused by the anisotropic parameter.

Let us consider now the contour C with the light-like direction $y_1^{\pm} = \frac{t \pm y_1}{\sqrt{2}}$. The metric in these coordinates has the form (60) with slightly different coefficients as compare to (61)

$$G_{--} = \frac{1}{2}\left(\frac{1}{z^{2/\nu}} - \frac{f}{z^2}\right), \quad G_{-+} = -\left(\frac{1}{z^{2/\nu} + \frac{f}{z^2}}\right), \tag{66}$$
$$G_{xx} = \frac{1}{z^2}, \quad G_{y_2y_2} = \frac{1}{z^{2/\nu}}, \quad G_{zz} = \frac{1}{z^2 f(z)}.$$

The small side of the contour C can be oriented in x or y_2 directions. In both cases the corresponding string actions have the form (63) and contain the metric coefficient G_{--} as in (66). This G_{--} is non-positive definite below horizon z_h, $0 < z < z_h$, for $\nu > 1$. This makes the string action (63) complex that one can interpret as a suppression of the jet quenching parameter.

4. Spatial Wilson loops in a time-dependent background

Now we move to consider the thermalization of rectangular Wilson loops in the Vaidya background (12)–(14), which describes collapsing geometry in the special anizotropic spacetime (1). We proceed in a similar manner as in the static case studying three possible configurations of spatial Wilson loops.

4.1. Wilson loops on the xy_1-plane

4.1.1. Rectangular strip infinite along the y_1-direction

As in Sec. 3 we start from the spatial rectangular Wilson loop on the xy_1-plane with the assumption that one side of the loop is infinite along the y_1-direction and the other has finite size along the x-direction (see (15)). Here we suppose the dependence $v = v(x)$, $z = z(x)$. The Nambu–Goto action takes the form similar to (18)

$$S_{x,y_{1(\infty)}} = L_y \int \frac{dx}{z^{1+\frac{1}{\nu}}}\sqrt{1 - f(z,v)v'^2 - 2v'z'}, \tag{67}$$

but with the time-dependent blackening function $f = f(z,v)$. The corresponding equations of motion are

$$v'' = \frac{1}{2}\frac{\partial f}{\partial z}v'^2 + \frac{(\nu+1)}{\nu z}(1 - fv'^2 - 2v'z'), \tag{68}$$
$$z'' = -\frac{\nu+1}{\nu}\frac{f}{z} + \frac{\nu+1}{\nu}\frac{f^2v'^2}{z} - \frac{1}{2}\frac{\partial f}{\partial v}v'^2 - \frac{1}{2}fv'^2\frac{\partial f}{\partial z} - v'z'\frac{\partial f}{\partial z} + 2\frac{(\nu+1)}{\nu z}fv'z',$$

which for $\nu = 1$ coincide with the Vaidya-AdS equations [17].

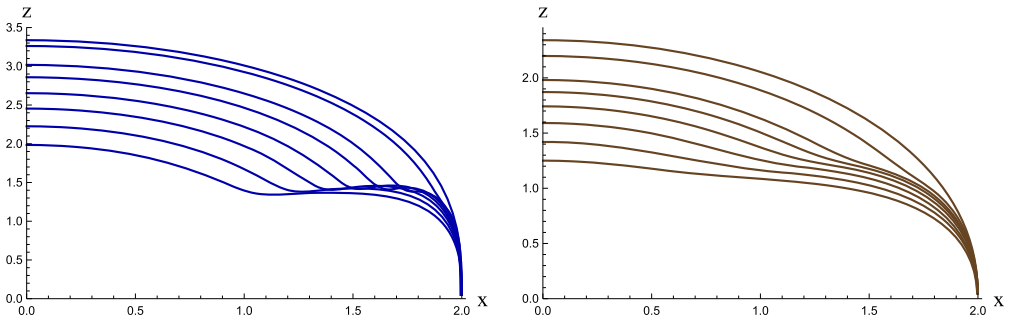

Fig. 5. Profiles of the string $z(x)$ (with the boundary condition $z(2) = 0$) at different moments of the boundary time $v = 1$ (left) and $v = 4$ (right). In (14) we take $m = 1$.

We have to consider eqs. (68) with the following boundary conditions $z(\pm\ell_x/2) = 0$, $v(\pm\ell_x/2) = t$, where ℓ_x is the length of the Wilson loop along the x-direction. To solve numerically the equations of motion (68), it is convenient to impose the initial conditions $z(0) = z_*$, $v(0) = v_*$, $z'(0) = 0$, $v'(0) = 0$.

Fig. 5 shows the typical behavior of the solutions to eqs. (68) which satisfy the boundary conditions for different values of the critical exponent ν. In these pictures we observe the evolution of string profiles during the formation of the black brane horizon by the infalling shell with $m = 1$.

For a given solution $(v(x), z(x))$ to eqs. (68) we can compute the functional for the Nambu–Goto action (67). We note that the dynamical system governed by (67) has the following integral of motion

$$\mathcal{J} = -\frac{1}{z^{1+1/\nu}\sqrt{\mathcal{R}}}, \tag{69}$$

where we denote

$$\mathcal{R} = 1 - f v'^2 - 2v'z'. \tag{70}$$

Taking into account (69)–(70) one can represent (67) in the following form

$$S_{x,y_{1(\infty)}} = L_y \int_0^{l_x} \frac{dx}{z^{1+1/\nu}} \left(\frac{z_*}{z}\right)^{1+1/\nu}, \tag{71}$$

where z_* is the turning point defined from the requirements $z' = v' = 0$ and related with $\mathcal{J}$ as $z_*^{1/\nu+1} = \mathcal{J}^{-1}$.

Coming to integration with respect to the z-variable the expression (71) can be represented as

$$S_{x,y_{1(\infty)},ren} = -L_{y_1} \int_{z_0}^{z_*} \frac{\mathfrak{b}(z)}{z^{1+1/\nu}} dz, \tag{72}$$

where $\mathfrak{b}$ is defined by

$$\mathfrak{b}(z) = \frac{1}{z'} \left(\frac{z_*}{z}\right)^{1+\frac{1}{\nu}}. \tag{73}$$

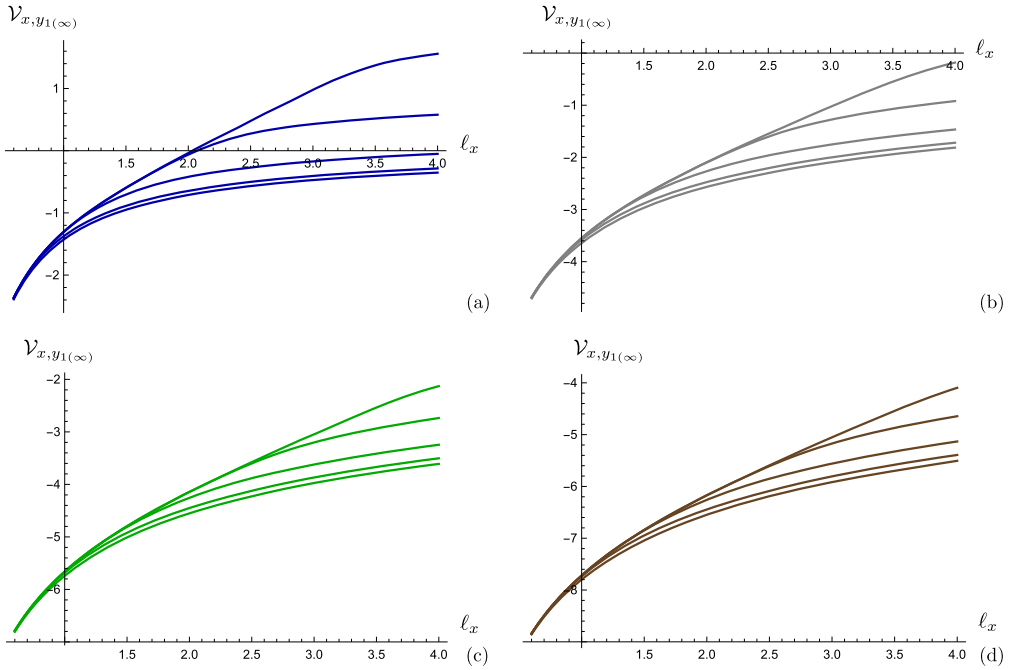

Fig. 6. The pseudopotential $\mathcal{V}_{x,y_{1(\infty)}}$ as a function of ℓ_x at fixed values of t for $\nu = 1, 2, 3, 4$ ((a), (b), (c), (d), respectively). Different curves correspond to time $t = 0.1, 0.5, 0.9, 1.4, 2$ (from down to top, respectively). In (14) we take $m = 1$.

One can observe that $\mathfrak{b}(z)$ tends to be -1 for $z \to 0$ and divergences at $z = 0$ are similar to the static configuration and by this reason we put the regularization z_0. Making a substraction we come to the renormalized version of $S_{x,y_{1(\infty)}}$, in which we can remove the regularization

$$S_{x,y_{1(\infty)},ren} = -L_{y_1}\left(\int_{z_0}^{z_*}\frac{[\mathfrak{b}(z)-\mathfrak{b}(z_0)]}{z^{1+1/\nu}}dz - \nu\frac{\mathfrak{b}(z_0)}{z_*^{1/\nu}}\right). \tag{74}$$

The pseudopotential is expressed as:

$$\mathcal{V}_{x,y_{1(\infty)}} = \frac{S_{x,y_{1(\infty)},ren}}{L_{y_1}}. \tag{75}$$

In Fig. 6 we present the behavior of the renormalized pseudopotential $\mathcal{V}_{x,y_{1(\infty)}}$ derived from the action (74) as a function of ℓ_x at fixed time moments for different values of ν. We see that for small distances the pseudopotential behaves similarly for different values of t. This dependence strengthens with increasing ν. For large times we see that the pseudopotential equilibrates to its thermal value. The pseudopotential reaches saturation for enough large size of the strip. The value of the thermalization time grows with increasing ℓ_x for all values of ν. At the same time, we observe that the saturation is reached faster for large ν.

4.1.2. Rectangular strip infinite along the x-direction

Now we consider the rectangular Wilson loop on the xy_1-plane with the assumption that its contour is infinite along the x-direction while it has finite stretch along the y_1-direction (see (16)).

As in the previous section, we specify this type of the strip by the subscript y_1, $x_{(\infty)}$. Thus, the corresponding Nambu–Goto action can be represented by

$$\frac{S_{y_1,\,x_{(\infty)}}}{L_x}=\int\frac{dy_1}{z^2}\sqrt{\frac{1}{z^{\frac{2}{\nu}-2}}-f(z,v)v'^2-2v'z'}, \tag{76}$$

with the notation $'\equiv\frac{d}{dy_1}$. The time-independent analogue of (76) is given by (36).

The equations of motion following from (76) are

$$\begin{aligned}
v''&=\frac{1}{2}\frac{\partial f}{\partial z}v'^2+\frac{\nu+1}{\nu z}\left(z^{2-2/\nu}-\frac{2\nu}{(1+\nu)}fv'^2-2v'z'\right), \\
z''&=-\frac{\nu+1}{\nu}fz^{1-2/\nu}+\frac{2(\nu-1)z'^2}{\nu}+\frac{2}{\nu}\frac{f^2v'^2}{z}-\frac{1}{2\nu}\frac{\partial f}{\partial v}v'^2 \\
&\quad-\frac{1}{2\nu}f\frac{\partial f}{\partial z}v'^2-z'v'\frac{\partial f}{\partial z}+\frac{4}{z}fz'v'.
\end{aligned} \tag{77}$$

It is worth to be noted that eqs. (77) match with (68) taken with $\nu=1$ and also reproduce those for the AdS-case.

The boundary conditions for eqs. (77) read $z(\pm\ell_{y_1}/2)=0,\quad v(\pm\ell_{y_1}/2)=t$, where ℓ_{y_1} is the length of the Wilson loop along the y_1-direction.

As in the previous case the action (76) can be simplified on equations of motions. For this purpose we note that the dynamical system governed by action (76) has the integral of motion

$$\mathcal{J}=-\frac{1}{z^{2/\nu}\sqrt{\mathcal{R}}}, \tag{78}$$

where

$$\mathcal{R}=\frac{1}{z^{2/\nu-2}}-fv'^2-2v'z'. \tag{79}$$

Taking into account (78)–(79) the action (76) is represented in the form

$$S_{y_1,\,x_{(\infty)}}=L_x\int\limits_0^{l_{y_1}}dy_1\frac{z_*^{1/\nu+1}}{z^{2/\nu+2}}, \tag{80}$$

with the turning point z_* related with $\mathcal{J}$ as $z_*^{1/\nu+1}=\mathcal{J}^{-1}$.

As in the previous case we present $S_{y_1,\,x_{(\infty)}}$ as

$$S_{y_1,\,x_{(\infty)}}=-L_x\int\limits_{z_0}^{z_*}\frac{\mathfrak{b}(z)}{z^2}dz, \tag{81}$$

where $\mathfrak{b}$ is defined by

$$\mathfrak{b}(z)=\frac{1}{z'}\left(\frac{z_*^{1+1/\nu}}{z^{2/\nu}}\right). \tag{82}$$

Performing renormalization we come to

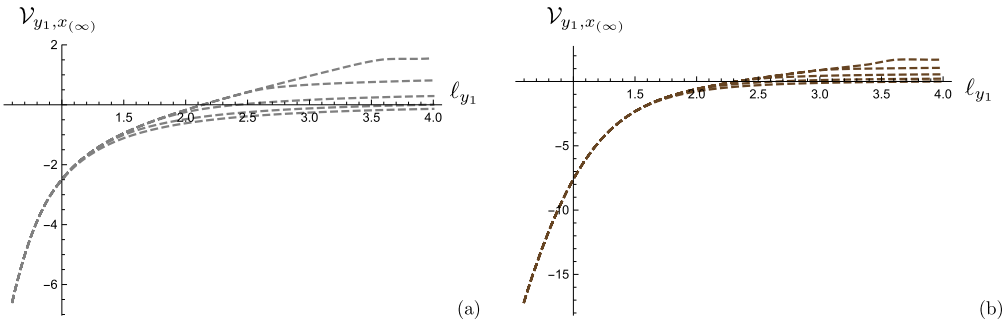

Fig. 7. The pseudopotential $\mathcal{V}_{y_1,x_{(\infty)}}$ as a function of ℓ_{y_1} at fixed values of t for $\nu = 2, 4$ ((a), (b) respectively). The plot for $\nu = 1$ is the same as in Fig. 6.a. Different curves correspond to $t = 0.1, 0.5, 0.9, 1.4, 2$ from down to top. In (14) we take $m = 1$.

$$S_{y_1,\,x_{(\infty)},ren} = -L_x \int_0^{z_*} \frac{\mathfrak{b}(z) - \mathfrak{b}(z_0)}{z^2} dz - \frac{\mathfrak{b}(z_0)}{z_*}. \tag{83}$$

The renormalized pseudopotential derived from the action (83) as a function of ℓ_{y_1} for different values of t and ν is demonstrated in Fig. 7. Here we again observe that for small ℓ_{y_1} the behavior of the pseudopotential is similar for different values of t. As in the previous case the behavior intensifies with the increasing value of the dynamical exponent. However, in contrast to the previous case there is no substantial dependence, on a given scale, of the thermalization time on the dynamical exponent. Comparing Fig. 6 and Fig. 7 one can see that for the same scale ℓ_{y_1} the thermalization of the Wilson loop occurs faster for the configuration with a long extent in the y_1-direction. The dependence on the dynamical exponent ν is also stronger for the latter case of the orientation.

4.2. *Wilson loop on the y_1y_2-plane*

Finally, we come to the configuration located on the y_1y_2-plane. We assume that this infinite rectangular strip is invariant along the y_2-direction, see (17). As in Sect. 3.2 we use y_1, $y_{2,(\infty)}$ for the subscript of the action

$$\frac{S_{y_1,\,y_{2,(\infty)}}}{L_{y_2}} = \int \frac{dy_1}{z^{1+\frac{1}{\nu}}} \sqrt{\frac{1}{z^{\frac{2}{\nu}-2}} - f v'^2 - 2v'z'}, \tag{84}$$

where we define $' \equiv \frac{d}{dy_1}$.

The equations of motion corresponding to (84) can be written down in the following form

$$\begin{aligned} v'' &= \frac{1}{2}\frac{\partial f}{\partial z} v'^2 + \frac{2}{z\nu}\left(z^{2-\frac{2}{\nu}} - \frac{\nu+1}{2} f v'^2 - 2v'z'\right), \\ z'' &= -\frac{2}{\nu} f z^{1-2/\nu} + 2\frac{\nu-1}{\nu}\frac{z'^2}{z} + \frac{\nu+1}{\nu z} f^2 v'^2 - \frac{1}{2}\frac{\partial f}{\partial v} v'^2 - \frac{1}{2} f \frac{\partial f}{\partial z} v'^2 \\ &\quad - z'v' \frac{\partial f}{\partial z} + \frac{2(\nu+1)}{\nu z} f v'z'. \end{aligned} \tag{85}$$

One can check that eqs. (85) coincide with (68) and (77) for $\nu = 1$ as well as come to be the equations for the AdS case. The boundary conditions to be satisfied by eqs. (85) have the stan-

dard form $z(\pm\ell_{y_1}/2)=0$, $v(\pm\ell_{y_1}/2)=t$, where ℓ_{y_1} is the length of the Wilson loop along the y_1-direction.

Following our strategy we compute the functional (84) on a given solution to (85). We note that the integral of motion for the configuration governed by the action (84) reads

$$\mathcal{J}=-\frac{1}{z^{\frac{3}{\nu}-1}\sqrt{\mathcal{R}}}, \tag{86}$$

where we define

$$\mathcal{R}=\frac{1}{z^{2/\nu-2}}-f(v')^2-2v'z'. \tag{87}$$

Plugging (86) into (84) we come to the following form for the functional of the Nambu–Goto action

$$S_{y_1,\,y_{2,(\infty)}}=L_{y_2}\int\limits_0^{l_{y_1}}dy_1\frac{z_*^{2/\nu}}{z^{4/\nu}}, \tag{88}$$

where the turning point z_* is related with $\mathcal{J}$ as $z_*^{2/\nu}=\mathcal{J}^{-1}$. Changing the variable of integration from y_1 to z we get

$$S_{y_1,\,y_{2,(\infty)}}=-L_{y_2}\int\limits_{z_0}^{z_*}\frac{\mathfrak{b}(z)}{z^{1+1/\nu}}dz, \tag{89}$$

where

$$\mathfrak{b}(z)=\frac{1}{z'}\left(\frac{z_*^{2/\nu}}{z^{3/\nu-1}}\right). \tag{90}$$

The renormalized action in terms of the z-variable reads

$$\frac{S_{y_1,\,y_{2,(\infty)},ren}}{L_{y_2}}=-\int\limits_{z_0}^{z_*}\frac{\mathfrak{b}(z)-\mathfrak{b}(z_0)}{z^{1+1/\nu}}dz+\nu\frac{\mathfrak{b}(z_0)}{z_*^{\frac{1}{\nu}}}. \tag{91}$$

Here the pseudopotential is expressed from (91) as:

$$\mathcal{V}_{y_1,\,y_{2(\infty)}}=\frac{S_{y_1,\,y_{2(\infty)},ren}}{L_{y_2}}. \tag{92}$$

The dependence of the pseudopotential $\mathcal{V}_{y_1,\,y_{2(\infty)}}$ on the length ℓ_{y_1} is shown in Fig. 8. As for the previous configurations of Wilson loop located on the xy_1-plane, the pseudopotential $\mathcal{V}_{y_1,\,y_{2(\infty)}}$ tends to its thermal value for large t. We note that the influence of the critical exponent on the rate of the thermalization process for $\mathcal{V}_{y_1,\,y_{2(\infty)}}$ is even higher than for $\mathcal{V}_{x,\,y_{1(\infty)}}$ and $\mathcal{V}_{y_1,\,x_{(\infty)}}$. In all these cases the saturation time increases with ℓ_{y_1} and ν.

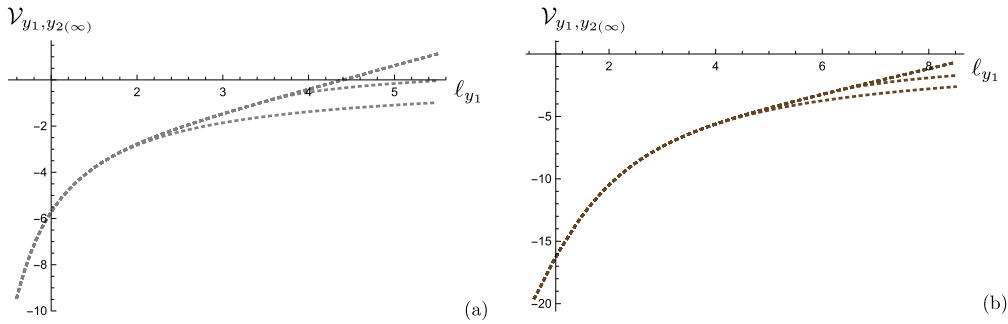

Fig. 8. The pseudopotential $\mathcal{V}_{y_1,\,y_{2(\infty)}}$ as a function of the length ℓ_{y_1} at fixed values of t, $\nu = 2, 4$ ((a), (b) respectively). (a): we take $t = 0.1, 0.5, 0.9, 1.4, 2$ from down to top, respectively; for plots (b): $t = 0.4, 1.5, 2.5, 3.34, 4$ from down to top, respectively. In (14) we take $m = 1$.

5. Thermalization times

5.1. Thermalization times of spatial Wilson loops

In this section, we compare the thermalization time for spatial Wilson loops with different orientations and its dependence on the value of the dynamical exponent ν. To simplify these estimations we consider the thin shell limit. We are interested in the value of the boundary time t_{therm} when the string profile is totally covered by the thin shell, i.e.:

$$t_{therm}(\ell) = \int_0^{z_*(\ell)} \frac{dz}{f(z)}, \tag{93}$$

where ℓ is the length between the string endpoints on the boundary given by (22),(40) or (51) for different orientations. In Fig. 9 we plot the dependence on ℓ of the thermalization time for two configurations in the xy_1-plane. In Fig. 10(a) the behavior of the thermalization time as a function of ℓ for the configuration in the transverse y_1y_2-plane is presented. One can see that the thermalization time decreases with increasing ν for all cases plotted in Fig. 9 and Fig. 10. The dependence on the length ℓ for the loop in the xy_1-plane with the short extent in the x-direction is linear. At the same time, the dependence for the loop in the same plane, but with the short extent in the y_1-direction, as well as for the loop in y_1y_2-plane, is not linear for small ℓ asymptoting to the linear dependence only for large ℓ. It should be noted that the deviation from linearity strengthens with increasing ν. We also see that for the configuration in the transverse plane, the deviation of the thermalization time for the anisotropic cases from the isotropic one the thermalization time is much stronger than for the other orientations. In Fig. 10(b) the comparison of thermalization times for different orientations in the case $\nu = 4$ is plotted. This plot shows that the dependence on the orientation is crucial, varying the orientation we change the order of thermalization time. This means that characteristic scale depends on the orientation. The similar behavior of the thermalization time on ℓ was observed for the thermalization time of two-point correlators in [53].

5.2. Thermalization times of different observables

It is interesting to compare the thermalization times of different observables. In our work [53] we have studied two-point correlation functions and the holographic entanglement entropy in the

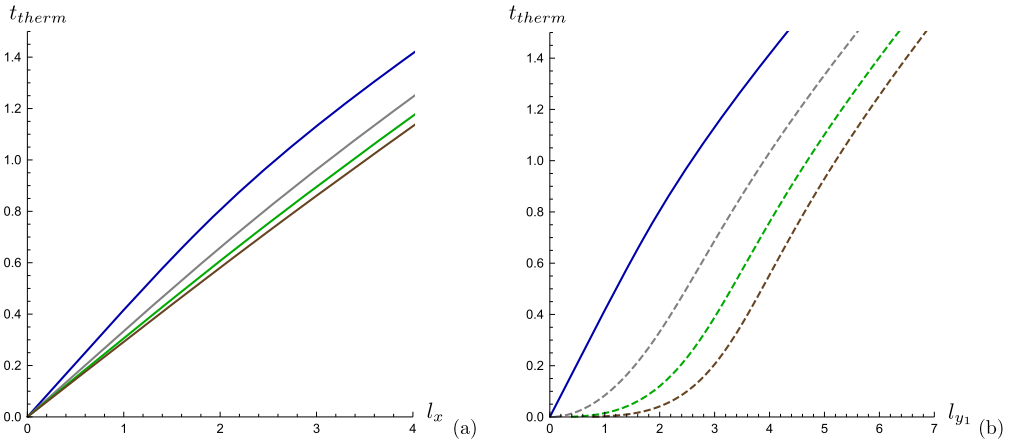

Fig. 9. The thermalization time for the Wilson loop in the xy_1-plane with a short extent in the x- and y-directions ((a) and (b), respectively). Different curves correspond to different values of $\nu = 1, 2, 3, 4$ (from top to down for each plot).

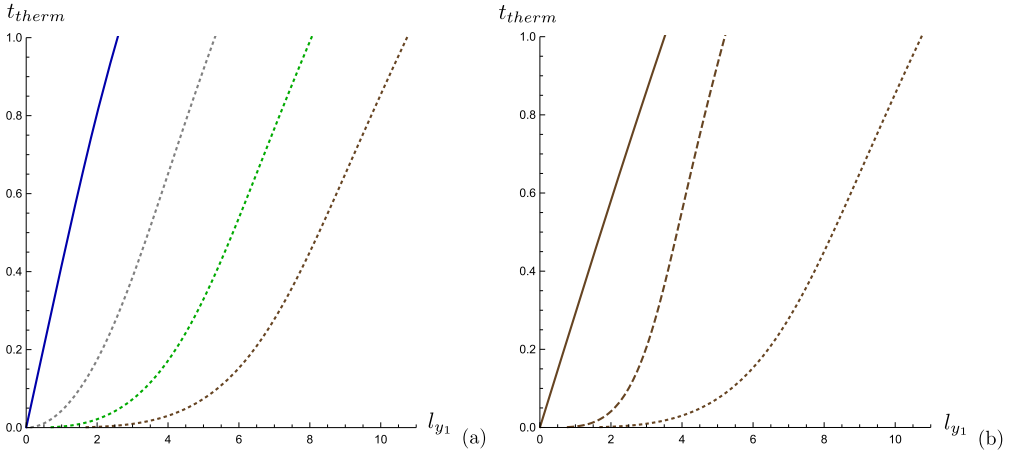

Fig. 10. (a)The thermalization time as a function of ℓ for the Wilson loop in the $y_1 y_2$-plane, different curves correspond to different values of $\nu = 1, 2, 3, 4$ (from left to right). (b) The thermalization time as a function of ℓ for $\nu = 4$, for Wilson loops with short extents in the x- and y-directions lying in the xy_1-plane and for the Wilson loop in the $y_1 y_2$-plane (from left to right).

Lifshitz-like backgrounds. By virtue of the spatial anisotropy of the metric we had two different configurations of the correlators and entropy with respect to the longitudinal and transversal directions. We have observed that the entanglement entropy for a subsystem delineated in the transversal direction thermalizes faster then the two-point correlator and Wilson loop in the longitudinal one. In [53] we also have calculated thermalization times for two-point correlators. In Appendix B the additional computations for the thermalization time of the holographic entanglement entropy are given. In Fig. 11 we show the comparison of the thermalization times for two point correlation functions, holographic entanglement entropy and Wilson loops for different configurations.

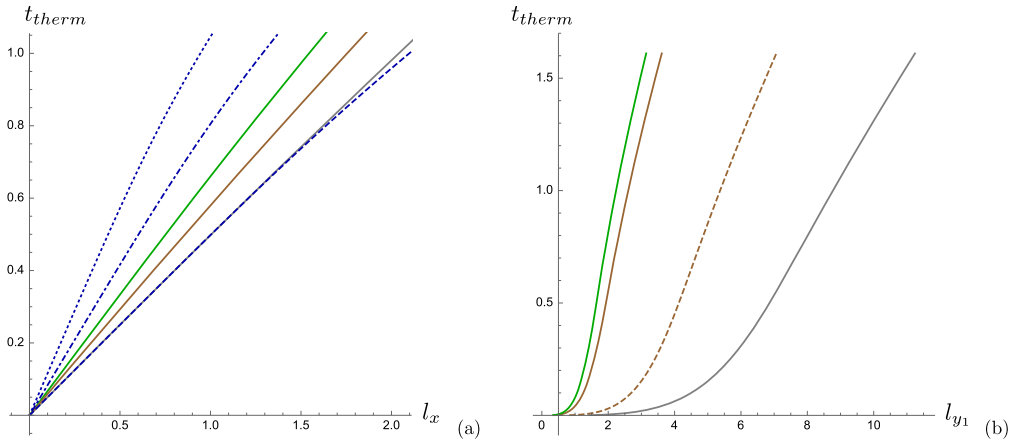

Fig. 11. The thermalization times of the two-point correlators, holographic entanglement entropy and Wilson loops for different configurations. (a) The solid lines (from left to right) correspond to the entropy(green), the Wilson loop (brown) and the two-point correlator (gray) with the dependences on the longitudinal direction x in the anisotropic background with $\nu = 4$, while the dashed, dash-dotted and dotted lines represent the behavior of the two-point correlator, Wilson loop and entropy in the isotropic spacetime, respectively. (b) The solid curves correspond to the entropy(green), the Wilson loop (brown) on the xy_1-plane and the two-point correlator (gray) with the dependences on the trasversal direction y_1. The dashed curve corresponds to the Wilson loop on the y_1y_2-plane. All plots in (b) are for the anisotropic background with $\nu = 4$.

We see that the order of the thermalization process in a certain direction is similar to the case in the isotropic and ordinary Lifshitz backgrounds [18]. The two-point correlator is the observable that thermalizes first, then we observe the thermalization of the Wilson loops, and the entanglement entropy is the observable that thermalizes last. One should be noted that the thermalization process of the Wilson loop and the entanglement entropy in the anisotropic background is faster even in the longitudinal direction than thermalization of the same observables in the isotropic case. From Fig. 11 (a) it is also interesting to see that the curves for the two-point correlator in the x-direction in the anisotropic background and the correlator in the isotropic spacetime match.

6. Conclusions

In this paper, we have explored the holographic scenario of the formation of the quark–gluon plasma using the bulk backgrounds (12), which possess spatially anisotropy. To probe the formation of the quark–gluon plasma we have used the rectangular spatial Wilson loops located on the boundary of our background (12). We have considered three possible configurations of Wilson loops on the boundary: the infinite rectangular strip located on the plane including one longitudinal and one transverse directions, the xy_1-plane, with a short extent in the x- or y_1-direction, and the infinite rectangular strip located on the transverse y_1y_2-plane.

We have analyzed Wilson loops both for static and time-dependent cases using the static black brane (9), and Vaidya solutions (12), respectively. The results obtained in this paper show how the expectations of Wilson loops are modified in the presence of anisotropy in the strong coupling limit.

We have found, that at small distances, the pseudopotential derived from the Wilson loop located in the xy_1-plane has a nontrivial dependence on the parameter ν. Namely, for $\nu > 1$ a breaking of the Coulomb phase has been observed. For Wilson loops lying in the transverse plane

the Coulomb phase is unbroken, and all dependence for small ℓ is encoded in the ν dependent constant. At large ℓ all pseudopotentials are linear growing functions. Also we have found that the magnetic string tension is also affected by the anisotropic parameter ν. For the contour located on the transverse directions, the dependence of the string tension on the temperature is suppressed by anisotropy, so the magnetic string tension becomes close to a constant value. This effect is clearly seen for large ν. We have also observed interesting results for Wilson loops in the Vaidya backgrounds (12). The effect of anisotropy parameter on the thermalization time for different orientations also has been investigated. In the $x, y_{1(\infty)}$-case of orientation the dependence of thermalization time on scale ℓ is linearly growing function for all ν. For other orientation the dependence is not linear. In the transverse orientation this can be seen very clear. Until some critical value the dependence is slowly growing function, and after this critical value it shows the linear growth.

A common feature in the behavior of the pseudopotential is the tendency of achievement of the saturation for large values of the boundary time. The dynamical exponent also influences to the thermalization of Wilson loops, so that the value of ν increases this behavior strengthens. We have seen that the thermalization is much faster than in the AdS case. It is worth noticing that the approach to the saturation also depends on the orientation of the Wilson loop. The configuration on the transversal directions the system saturates quicker than for the contours on the xy_1-plane.

Comparing to results for the evolution of the holographic entanglement entropy in the backgrounds (12) in [53] we have found that the thermalization process both of the Wilson loops and the entanglement entropy is faster in the transverse direction. We have seen the similar behavior of the thermalization time as a function of ℓ for the two-point correlators in [53].

We also calculated the dependence of the jet quenching parameter on the orientation and on the anisotropic parameter ν. We also noticed that for special orientations the string action defined the jet quenching parameter becomes complex that leads to a suppression of the jet quenching parameter. This phenomena requires more elaborations as well as the study of the time evolution of the jet quenching parameter modeling by the light-like Wilson loop in the time-depending background (12).

It would be interesting to generalize our results to the case of the modified backgrounds that describe confinement/deconfinement phase transition [69].

Acknowledgements

We are grateful to Oleg Andreev and Oleg Teryaev for useful discussions.

Appendix A. Asymptotics for static pseudopotentials

Here we collect the expressions for asymptotics of static pseudopotentials.

A.1. Rectangular strip in xy_1-plane infinite along the y_1-direction

The integral in (26) can be evaluated approximately

$$\ell_x \approx -\frac{\sqrt{\pi} z_* \Gamma\left(-\frac{1}{2\nu+2}\right)(6\nu+4+(2\nu+1)m z_*^{\frac{2}{\nu}+2})}{2(\nu+1)(3\nu+2)\Gamma\left(\frac{\nu}{2\nu+2}\right)}. \tag{A.1}$$

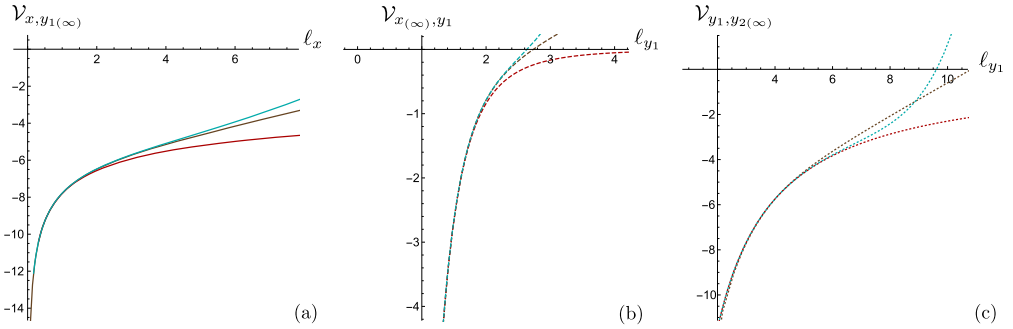

Fig. 12. a) The comparison of the pseudopotentials given by exact formula (25) (the brown line), massless approximation (the red bottom line) and the first massive correction (the cyan top line) (A.4). b) The comparison of the pseudopotentials given by exact formula (84) (the brown dashed line), massless approximation (the red bottom dashed line) and the first massive correction (the cyan top dashed line) (A.7). c) The comparison of the pseudopotentials given by exact formula (48) (the brown dotted line), massless approximation (the red bottom dotted line) and the first massive correction (the cyan top dotted line) (A.11). For all plots $m = 0.2$.

For $\nu = 4$ we have

$$84\ell_x \approx 5.12 z_* \left(28 + 9 m z_*^{5/2}\right)$$

and this gives

$$z_* = \ell_x \left(0.586 - 0.0495 \ell_x^{5/2} m + \mathcal{O}(\ell_x^5 m^2)\right). \tag{A.2}$$

Evaluating (25) for $\nu = 4$ we get approximately

$$\mathcal{V}_{x,y_{1(\infty)}} = -\frac{\frac{8\sqrt{\pi}\Gamma\left(\frac{9}{10}\right)}{\Gamma\left(\frac{2}{5}\right)} + \frac{\sqrt{\pi}\Gamma\left(\frac{9}{10}\right)}{\Gamma\left(\frac{2}{5}\right)} m z_*^{5/2} + \mathcal{O}\left(m^2 z_*^5\right)}{z_*^{1/4}}. \tag{A.3}$$

Substituting (A.2) in (A.3) we get

$$\mathcal{V}_{x,y_{1(\infty)}} = -\frac{7.80}{l_x^{1/4}} \left(1 - 0.012\, m\, l_x^{5/2} + \mathcal{O}\left(m^2 l_x^5\right)\right) \tag{A.4}$$

In Fig. 12 we present the comparison of the pseudopotentials given by exact formula (25), (26) and the approximated formula (A.4).

Inverting (A.1) for arbitrary ν we obtain

$$z_* = l_x \left(\frac{\Gamma\left(\frac{\nu}{2\nu+2}\right)}{2\sqrt{\pi}\Gamma\left(1 - \frac{1}{2(\nu+1)}\right)} - B_{l_x} m l_x^{\frac{2}{\nu}+2} + \mathcal{O}(\ell_x^{\frac{4}{\nu}+4} m^2)\right),$$

where

$$B_{l_x} = \frac{\nu \left(\frac{\Gamma\left(\frac{\nu}{2\nu+2}\right)}{\Gamma\left(1-\frac{1}{2(\nu+1)}\right)}\right)^{\frac{2}{\nu}+4} \Gamma\left(2 - \frac{1}{2(\nu+1)}\right)}{(\nu+1) 2^{\frac{2}{\nu}+5} \pi^{\frac{1}{\nu}+\frac{3}{2}} \Gamma\left(\frac{5\nu+4}{2\nu+2}\right)}.$$

The pseudopotential $\mathcal{V}_{x,y_{1(\infty)}}$ can be evaluated approximately

$$\mathcal{V}_{x,y_{1(\infty)}} = l_x^{-\frac{1}{\nu}} \left(A_{l_x} + F_{l_x}\, m\, l_x^{\frac{2}{\nu}+2} + \mathcal{O}(m^2\, l_x^{\frac{4}{\nu}+4}) \right),$$

where

$$A_{l_x} = \frac{\nu^2 \Gamma\left(-\frac{1}{2(\nu+1)}\right) \Gamma\left(1-\frac{1}{2(\nu+1)}\right)^{\frac{1}{\nu}} \left(\Gamma\left(\frac{\nu}{2\nu+2}\right)\right)^{-1/\nu}}{2^{2-\frac{1}{\nu}} \pi^{\frac{\nu+1}{2\nu}-\frac{1}{\nu}-1} (\nu+1)^2 \Gamma\left(\frac{3\nu+2}{2\nu+2}\right)},$$

$$F_{l_x} = \frac{\csc\left(\frac{\pi}{2\nu+2}\right) \Gamma\left(\frac{-1}{2(\nu+1)}\right) \Gamma\left(\frac{2(\nu+1)-1}{2(\nu+1)}\right)^{-\frac{1+3\nu}{\nu}} \Gamma\left(\frac{\nu}{2\nu+2}\right)^{\frac{2\nu+1}{\nu}}}{2^{\frac{1}{\nu}+3} \pi^{\frac{\nu+1}{2\nu}-1} (\nu+2) \Gamma\left(\frac{1}{2\nu+2}\right) \Gamma\left(-\frac{\nu+2}{2\nu+2}\right)}$$

$$+ \frac{\Gamma\left(\frac{-1}{2(\nu+1)}\right) \Gamma\left(\frac{3\nu+2}{2\nu+2}\right) \Gamma\left(\frac{4(\nu+1)-1}{2(\nu+1)}\right) \Gamma\left(\frac{\nu}{2\nu+2}\right)^{\frac{1}{\nu}+2}}{(\nu+2) 2^{\frac{1}{\nu}+3} \pi^{\frac{\nu+1}{2\nu}} \Gamma\left(-\frac{\nu+2}{2\nu+2}\right) \Gamma\left(\frac{5\nu+4}{2\nu+2}\right) \Gamma\left(\frac{2(\nu+1)-1}{2(\nu+1)}\right)^{\frac{1+3\nu}{\nu}}}.$$

For large ν one can expand the coefficients and obtain

$$\frac{\ell_x^{1/\nu}}{2\nu\left(1-\frac{\pi^2}{24\nu^2}\right)} \mathcal{V}_{x,y_{1(\infty)}} = -1 - + \frac{1+3\nu}{3\left(24\nu^2-\pi^2\right)}\, m\, \ell_x^{\frac{2}{\nu}+2} + \mathcal{O}(m^2\, \ell_x^{\frac{4}{\nu}+4}).$$

A.2. Rectangular strip in the xy_1-plane infinite along the x-direction

For $\nu = 4$ the integral (40) can be evaluate approximately

$$\frac{\ell_{y_1}}{z_*^{1/4}} = \frac{22 \cdot 2^{4/5} \pi \Gamma\left(\frac{6}{5}\right)}{5\Gamma\left(\frac{1}{10}\right)\Gamma\left(\frac{21}{10}\right)} + \frac{6 \cdot 2^{4/5} \pi \Gamma\left(\frac{6}{5}\right)}{5\Gamma\left(\frac{1}{10}\right)\Gamma\left(\frac{21}{10}\right)} z_*^{5/2} + \mathcal{O}\left(m^2 z_*^5\right)$$

and inverting we get

$$z_* = \ell_{y_1}^4 \left[0.0412 - 0.0000155 m\, \ell_{y_1}^{10} + \mathcal{O}\left(m^2 {l_2}^{20}\right) \right]. \tag{A.5}$$

The pseudopotential for $\nu = 4$ reads

$$\mathcal{V}_{y_1,\, x_{(\infty)}}(z_*) = \frac{-2\frac{\sqrt{\pi}\Gamma\left(\frac{3}{5}\right)}{\Gamma\left(\frac{1}{10}\right)} + 4\frac{\sqrt{\pi}\Gamma\left(\frac{3}{5}\right)}{\Gamma\left(\frac{1}{10}\right)} m z_*^{5/2} + \mathcal{O}(m^2 z_*^5)}{z_*}. \tag{A.6}$$

Plugging (A.5) in (A.6) we get

$$\mathcal{V}_{y_1,\, x_{(\infty)}}(\ell_{y_1}) = -\frac{13.5}{\ell_{y_1}^4} \left(1 - 0.00031 m \ell_{y_1}^{10} + \mathcal{O}(m^2 \ell_{y_1}^{20})\right). \tag{A.7}$$

Performing the same for arbitrary ν we have

$$\frac{z_*}{l_y^\nu} = \left(\frac{2\,\pi^{1/2} \Gamma\left(\frac{1}{2\nu+2}\right)}{\nu\Gamma\left(\frac{\nu+2}{2\nu+2}\right)} \right)^\nu - \frac{\nu(\nu+2) \left(\frac{\Gamma\left(\frac{1}{2\nu+2}\right)}{\nu\Gamma\left(\frac{\nu+2}{2\nu+2}\right)} \right)^{3\nu+2}}{8^{\nu+1} \pi^{\frac{3\nu}{2}+1} (2\nu+3)} m \ell_{y_1}^{2\nu+2} + O(m^2 \ell_{y_1}^{4\nu+4})$$

and

$$\mathcal{V}_{y_1,\,x_{(\infty)}}(\ell_{y_1}) = \frac{Q_{l_y} + C_{l_y} m \ell_{y_1}^{2+2\nu} + \mathcal{O}(m^2 \ell_{y_1}^{4+4\nu})}{\ell_{y_1}^{\nu}}, \tag{A.8}$$

where

$$Q_{l_y} = \frac{2^{\nu} \pi^{\frac{\nu+1}{2}} \nu^{\nu+1} \Gamma\left(-\frac{\nu}{2\nu+2}\right) \Gamma\left(\frac{\nu+2}{2\nu+2}\right)^{\nu}}{(\nu+1)\Gamma\left(\frac{1}{2\nu+2}\right)^{\nu+1}},$$

$$C_{l_y} = -\frac{\Gamma\left(\frac{1}{2\nu+2}\right)^{\nu+1} \Gamma\left(-\frac{\nu}{2\nu+2}\right) \Gamma\left(\frac{\nu+2}{2\nu+2}\right)^{-\nu-2}}{2^{\nu+3} \nu^{\nu} \pi^{\frac{\nu}{2}+\frac{1}{2}} (2\nu+3)}.$$

For large ν we have the expansion for (A.8)

$$\ell_{y_1}^{\nu} \mathcal{V}_{y_1,\,x_{(\infty)}}(\ell_{y_1}) = -2\pi^{1/2+\nu} + \frac{(2\nu-1) e^{\frac{24\nu-\pi^2+12}{24\nu}}}{4\pi^{\nu+1}\nu} m \ell_{y_1}^{2+2\nu} + \mathcal{O}(m^2 \ell_{y_1}^{4+4\nu}).$$

A.3. Rectangular strip in $y_1 y_2$-plane infinite along the y_2-direction

For $\nu = 4$ the integral (53) can be evaluated approximately

$$\frac{\ell_{y_1}}{z_*^{1/4}} = \frac{2\sqrt{\pi}\Gamma\left(\frac{3}{4}\right)}{\Gamma\left(\frac{5}{4}\right)} + \frac{\sqrt{\pi}\Gamma\left(\frac{13}{4}\right)}{\Gamma\left(\frac{15}{4}\right)} m z_*^{5/2} + \mathcal{O}(m^2 z_*^{10})$$

and this gives

$$z_* = \ell_{y_1}^4 \left(0.00190 - 2.52\ 10^{-10} m \ell_{y_1}^{10} + \mathcal{O}\left(m^2 \ell_{y_1}^{20}\right)\right). \tag{A.9}$$

The pseudopotential for $\nu = 4$

$$\mathcal{V}_{y_1,\,y_{2(\infty)}}(z_*) = \frac{\frac{2\sqrt{\pi}\Gamma\left(-\frac{1}{4}\right)}{\Gamma\left(\frac{1}{4}\right)} + \frac{\sqrt{\pi}\Gamma\left(\frac{9}{4}\right) m z_*^{5/2}}{\Gamma\left(\frac{11}{4}\right)} + \mathcal{O}(m^2 z_*^5)}{z_*^{1/4}}. \tag{A.10}$$

Substituting (A.9) in (A.10) we get

$$\mathcal{V}_{y_1,\,y_{2(\infty)}} = -\frac{23.0\left(1 - 0.741 \cdot 10^{-9} m\, \ell_{y_1}^{10} + \mathcal{O}\left(m^2 \ell_{y_1}^{20}\right)\right)}{\ell_{y_1}}. \tag{A.11}$$

For an arbitrary value of ν from (53) we have

$$z_* = \ell_{y_1}^{\nu} \left[C_1 + C_2 m \ell_{y_1}^{2\nu+2} + \mathcal{O}(m^2 \ell_{y_1}^{4+4\nu})\right], \tag{A.12}$$

where

$$C_1 = 2^{-\nu} \nu^{-\nu} \pi^{-\nu/2} \left(\frac{\Gamma\left(\frac{1}{4}\right)}{\Gamma\left(\frac{3}{4}\right)}\right)^{\nu}$$

$$C_2 = -\frac{2^{-3\nu-5} \nu^{-3\nu-1} \pi^{-\frac{3\nu}{2}-1} \Gamma\left(\frac{1}{4}\right)^{3\nu+3} \Gamma\left(\frac{\nu}{2}+\frac{5}{4}\right)}{\Gamma\left(\frac{\nu}{2}+\frac{7}{4}\right) \Gamma\left(\frac{3}{4}\right)^{3\nu+3}}$$

The pseudopotential for general ν can expressed as

$$\frac{4\mathcal{V}_{y_1,\,y_{2(\infty)}}(z_*)}{\sqrt{\pi}\nu z_*^{-1/\nu}} = \frac{2\Gamma\left(-\frac{1}{4}\right)}{\Gamma\left(\frac{1}{4}\right)} + \frac{m\Gamma\left(\frac{\nu}{2}+\frac{1}{4}\right)z_*^{\frac{2}{\nu}+2}}{\Gamma\left(\frac{1}{4}(2\nu+3)\right)} + \mathcal{O}(m^2 z_*^{4+4/\nu}). \tag{A.13}$$

Plugging (A.12) in (A.13) we get the following formula for the pseudopotential for large ν

$$\ell_{y_1}\mathcal{V}_{y_1,\,y_{2(\infty)}}(\ell_{y_1}) = -\frac{4\pi\nu^2\Gamma\left(\frac{3}{4}\right)^2}{\Gamma\left(\frac{1}{4}\right)^2} + \frac{\Gamma\left(\frac{1}{4}\right)^{2\nu+1}\Gamma\left(\frac{3}{4}\right)^{-2\nu-1}}{2^{2\nu+\frac{5}{2}}\nu^{2\nu+\frac{3}{2}}\pi^{\nu}} m\ell_{y_1}^{2\nu+2} + O(m^2\ell_{y_1}^{4+4\nu}).$$

Appendix B. Thermalization times of holographic two-point correlators and entanglement entropy

B.1. Thermalization time of two-point correlators

Under the holographic approach one can find the thermalization time t_{therm} of the two-point correlator at the scale ℓ using the Vaidya background. For this, one should consider a geodesic of a bulk particle with equal time endpoints located at the distance ℓ and find the time when the geodesic covered by the shell. In the Vaidya–Lifshitz background (12)–(13) we should study the thermalization in both longitudinal and transversal directions.

For the thermalization in the longitudinal direction we have the following relation for the length

$$\ell_x = 2z_* \int_0^1 \frac{w dw}{\sqrt{f(z_* w)(1-w^2)}},$$

where $w = z/z_*$ and the turning point is assumed to lie above the horizon, i.e. $z_h > z_*$.

The distance in the transversal direction is given by

$$\ell_{y_1} = 2z_*^{1/\nu} \int_0^1 \frac{w^{-1+2/\nu} dw}{\sqrt{f(w z_*)(1-w^{2/\nu})}}.$$

The thermalization time of the two-point correlator in both directions is defined by

$$t_{therm} = z_* \int_0^1 \frac{dw}{f(z_* w)}. \tag{B.1}$$

B.2. Thermalization time of entanglement entropy

To study the thermalization of the entanglement entropy we should also consider configurations in the longitudinal and transversal directions.

The longitudinal length scale is given by

$$\ell_x = 2\int_0^1 z_* w^{1+2/\nu} \frac{dw}{\sqrt{f(z_* w)(1-w^{2(1+2/\nu)})}}. \tag{B.2}$$

The length for a subsystem delineated in the transversal direction is

$$\ell_{y_1} = 2z_*^{1/\nu} \int_0^1 \frac{w^{3/\nu} dw}{\sqrt{f(w, z_*)(1 - w^{2(1+2/\nu)})}}.$$

Here we are also interested in the value of the boundary time when the surface is covered by the shell, i.e. the thermalization time of the entanglement entropy has the same expression as for the two-point correlator (B.1).

References

[1] K.G. Wilson, Confinement of quarks, Phys. Rev. D 10 (1974) 2445.
[2] I.Y. Arefeva, Quantum contour field equations, Phys. Lett. B 93 (1980) 347.
[3] J. Casalderrey-Solana, H. Liu, D. Mateos, K. Rajagopal, U.A. Wiedemann, Gauge/string duality, hot QCD and heavy ion collisions, arXiv:1101.0618.
[4] O. DeWolfe, S.S. Gubser, C. Rosen, D. Teaney, Heavy ions and string theory, Prog. Part. Nucl. Phys. 75 (2014) 86, arXiv:1304.7794.
[5] I.Ya. Aref'eva, Holographic approach to quark–gluon plasma in heavy ion collisions, Phys. Usp. 57 (2014) 527.
[6] S.S. Gubser, S.S. Pufu, A. Yarom, Entropy production in collisions of gravitational shock waves and of heavy ions, Phys. Rev. D 78 (2008) 066014, arXiv:0805.1551.
[7] J.L. Albacete, Y.V. Kovchegov, A. Taliotis, Modeling heavy ion collisions in AdS/CFT, J. High Energy Phys. 07 (2008) 100, arXiv:0805.2927.
[8] L. Alvarez-Gaume, C. Gomez, A. Sabio Vera, A. Tavanfar, M.A. Vazquez-Mozo, Critical formation of trapped surfaces in the collision of gravitational shock waves, J. High Energy Phys. 02 (2009) 009, arXiv:0811.3969.
[9] P.M. Chesler, L.G. Yaffe, Horizon formation and far-from-equilibrium isotropization in supersymmetric Yang–Mills plasma, Phys. Rev. Lett. 102 (2009) 211601, arXiv:0812.2053.
[10] S. Lin, E. Shuryak, Grazing collisions of gravitational shock waves and entropy production in heavy ion collision, Phys. Rev. D 79 (2009) 124015, arXiv:0902.1508.
[11] I.Ya. Aref'eva, A.A. Bagrov, E.A. Guseva, Critical formation of trapped surfaces in the collision of non-expanding gravitational shock waves in de Sitter space–time, J. High Energy Phys. 12 (2009) 009, arXiv:0905.1087.
[12] P.M. Chesler, L.G. Yaffe, Holography and colliding gravitational shock waves in asymptotically AdS5 spacetime, Phys. Rev. Lett. 106 (2011) 021601, arXiv:1011.3562.
[13] I.Ya. Aref'eva, A.A. Bagrov, E.O. Pozdeeva, Holographic phase diagram of quark–gluon plasma formed in heavy-ions collisions, J. High Energy Phys. 05 (2012) 117, arXiv:1201.6542.
[14] E. Kiritsis, A. Taliotis, Multiplicities from black-hole formation in heavy-ion collisions, J. High Energy Phys. 04 (2012) 065, arXiv:1111.1931.
[15] I.Ya. Aref'eva, E.O. Pozdeeva, T.O. Pozdeeva, Holographic estimation of multiplicity and membranes collision in modified spaces AdS_5, Theor. Math. Phys. 176 (2013) 861, arXiv:1401.1180v1.
[16] P. Vaidya, The external field of a radiating star in general relativity, Curr. Sci. 12 (1943) 183.
[17] V. Balasubramanian, A. Bernamonti, J. de Boer, N. Copland, B. Craps, E. Keski-Vakkuri, B. Muller, A. Schafer, et al., Holographic thermalization, Phys. Rev. D 84 (2011) 026010, arXiv:1103.2683.
[18] V. Keranen, E. Keski-Vakkuri, L. Thorlacius, Thermalization and entanglement following a non-relativistic holographic quench, Phys. Rev. D 85 (2012) 026005, arXiv:1110.5035.
[19] I.Ya. Aref'eva, I.V. Volovich, On holographic thermalization and dethermalization of quark–gluon plasma, arXiv:1211.6041.
[20] M. Strickland, Thermalization and isotropization in heavy-ion collisions, Pramana 84 (2015) 671, arXiv:1312.2285.
[21] D. Giataganas, Observables in strongly coupled anisotropic theories, PoS Corfu 2012 (2013) 122, arXiv:1306.1404.
[22] J.M. Maldacena, Wilson loops in large N field theories, Phys. Rev. Lett. 80 (1998) 4859–4862, arXiv:hep-th/9803002.
[23] S.J. Rey, S. Theisen, J.T. Yee, Wilson–Polyakov loop at finite temperature in large N gauge theory and anti-de Sitter supergravity, Nucl. Phys. B 527 (1998) 171, arXiv:hep-th/9803135.
[24] A. Brandhuber, N. Itzhaki, J. Sonnenschein, S. Yankielowicz, Wilson loops in the large N limit at finite temperature, Phys. Lett. B 434 (1998) 36, arXiv:hep-th/9803137.
[25] J. Sonnenschein, What does the string/gauge correspondence teach us about Wilson loops?, arXiv:hep-th/0003032.

[26] J. Babington, J. Erdmenger, N.J. Evans, Z. Guralnik, I. Kirsch, Chiral symmetry breaking and pions in non-supersymmetric gauge/gravity duals, Phys. Rev. D 69 (2004) 066007, arXiv:hep-th/0306018.
[27] M. Kruczenski, D. Mateos, R.C. Myers, D.J. Winters, Towards a holographic dual of large N(c) QCD, J. High Energy Phys. 05 (2004) 041, arXiv:hep-th/0311270.
[28] T. Sakai, S. Sugimoto, More on a holographic dual of QCD, Prog. Theor. Phys. 114 (2006) 1083, arXiv:hep-th/0507073.
[29] J. Polchinski, M.J. Strassler, Deep inelastic scattering and gauge/string duality, J. High Energy Phys. 05 (2003) 012, arXiv:hep-th/0209211.
[30] A. Karch, E. Katz, D.T. Son, M.A. Stephanov, Linear confinement and AdS/QCD, Phys. Rev. D 74 (2006) 015005, arXiv:hep-ph/0602229.
[31] O. Andreev, V.I. Zakharov, Heavy-quark potentials and AdS/QCD, Phys. Rev. D 74 (2006) 025023, arXiv:hep-ph/0604204.
[32] C.D. White, The Cornell potential from general geometries in AdS/QCD, Phys. Lett. B 652 (2007) 79, arXiv:hep-ph/0701157.
[33] U. Gursoy, E. Kiritsis, L. Mazzanti, F. Nitti, Holography and thermodynamics of 5D dilaton-gravity, J. High Energy Phys. 05 (2009) 033, arXiv:0812.0792.
[34] B. Galow, E. Megias, J. Nian, H.J. Pirner, Phenomenology of AdS/QCD and its gravity dual, Nucl. Phys. B 834 (2010) 330, arXiv:0911.0627.
[35] S. He, M. Huang, Q.-S. Yan, Logarithmic correction in the deformed AdS_5 model to produce the heavy quark potential and QCD beta function, Phys. Rev. D 83 (2011) 045034, arXiv:1004.1880.
[36] U. Gursoy, E. Kiritsis, L. Mazzanti, G. Michalogiorgakis, F. Nitti, Improved holographic QCD, Lect. Notes Phys. 828 (2011) 79, arXiv:1006.5461.
[37] D.S. Ageev, I.Y. Aref'eva, Holographic thermalization in a quark confining background, J. Exp. Theor. Phys. 120 (3) (2015) 436, arXiv:1409.7558.
[38] T. Andrade, Y. Lei, S.F. Ross, Scattering amplitudes in Lifshitz spacetime, Class. Quantum Gravity 31 (21) (2014) 215002, arXiv:1406.6389.
[39] T.R. Araujo, H. Nastase, Non-Abelian T-duality for nonrelativistic holographic duals, J. High Energy Phys. 11 (2015) 203, arXiv:1508.06568.
[40] D. Giataganas, Probing strongly coupled anisotropic plasma, J. High Energy Phys. 07 (2012) 031, arXiv:1202.4436.
[41] M. Chernicoff, D. Fernandez, D. Mateos, D. Trancanelli, Jet quenching in a strongly coupled anisotropic plasma, J. High Energy Phys. 08 (2012) 041, arXiv:1203.0561.
[42] A. Rebhan, D. Steineder, Probing two holographic models of strongly coupled anisotropic plasma, J. High Energy Phys. 08 (2012) 020, arXiv:1205.4684.
[43] P. Fonda, L. Franti, V. Keranen, E. Keski-Vakkuri, L. Thorlacius, E. Tonni, Holographic thermalization with Lifshitz scaling and hyperscaling violation, J. High Energy Phys. 08 (2014) 051, arXiv:1401.6088.
[44] T.R. Araujo, Revisiting Wilson loops for nonrelativistic backgrounds, Phys. Rev. D 92 (2015) 126007, arXiv:1509.0201.
[45] H. Liu, K. Rajagopal, U.A. Wiedemann, Calculating the jet quenching parameter from AdS/CFT, Phys. Rev. Lett. 97 (2006) 182301, arXiv:hep-ph/0605178.
[46] H. Liu, K. Rajagopal, U.A. Wiedemann, Wilson loops in heavy ion collisions and their calculation in AdS/CFT, J. High Energy Phys. 03 (2007) 066, arXiv:hep-ph/0612168.
[47] I.Ya. Aref'eva, A.A. Golubtsova, Shock waves in Lifshitz-like spacetimes, J. High Energy Phys. 1504 (2015) 011, arXiv:1410.4595.
[48] M. Taylor, Non-relativistic holography, arXiv:0812.0530.
[49] T. Azeyanagi, W. Li, T. Takayanagi, On string theory duals of Lifshitz-like fixed points, J. High Energy Phys. 06 (2009) 084, arXiv:0905.0688.
[50] D. Mateos, D. Trancanelli, Thermodynamics and instabilities of a strongly coupled anisotropic plasma, J. High Energy Phys. 07 (2011) 054, arXiv:1106.1637.
[51] S. Kachru, X. Liu, M. Mulligan, Gravity duals of Lifshitz-like fixed points, Phys. Rev. D 78 (2008) 106005, arXiv:0808.1725.
[52] I.Ya. Aref'eva, Formation time of quark–gluon plasma in heavy-ion collisions in the holographic shock wave model, Theor. Math. Phys. 184 (3) (2015) 1239–1255, arXiv:1503.02185.
[53] I.Y. Aref'eva, A.A. Golubtsova, E. Gourgoulhon, Analytic black branes in Lifshitz-like backgrounds and thermalization, J. High Energy Phys. 09 (2016) 142, arXiv:1601.06046.
[54] A. Hajilou, M. Ali-Akbari, F. Charmchi, A classical string in Lifshitz–Vaidya geometry, arXiv:1707.00967.
[55] M. Ali-Akbari, F. Charmchi, A. Davody, H. Ebrahim, L. Shahkarami, Evolution of Wilson loop in time-dependent N=4 super Yang–Mills plasma, Phys. Rev. D 93 (8) (2016) 086005, arXiv:1510.00212.

[56] I.Y. Arefeva, Large N QCD at high-energies as two-dimensional field theory, Phys. Lett. B 328 (1994) 411, arXiv:hep-th/9306014.
[57] I. Arefeva, Non-Abelian Stokes formula, Theor. Math. Phys. 43 (1980) 353.
[58] G.S. Bali, J. Fingberg, U.M. Heller, F. Karsch, K. Schilling, The spatial string tension in the deconfined phase of the $(3+1)$-dimensional SU(2) gauge theory, Phys. Rev. Lett. 71 (1993) 3059, arXiv:hep-lat/9306024.
[59] P. Petreczky, Lattice QCD at non-zero temperature, J. Phys. G 39 (2012) 093002, arXiv:1203.5320.
[60] A. Simonov, http://195.178.214.34/ps/1248/article_18874.pdf.
[61] J. Alanen, K. Kajantie, V. Suur-Uski, Spatial string tension of finite temperature QCD matter in gauge/gravity duality, Phys. Rev. D 80 (2009) 075017, arXiv:0905.2032.
[62] O. Andreev, V.I. Zakharov, The spatial string tension, thermal phase transition, and AdS/QCD, Phys. Lett. B 645 (2007) 437, arXiv:hep-ph/0607026.
[63] O. Andreev, The spatial string tension in the deconfined phase of SU(N) gauge theory and gauge/string duality, Phys. Lett. B 659 (2008) 416, arXiv:0709.4395.
[64] O. Andreev, Some multi-quark potentials, pseudo-potentials and AdS/QCD, Phys. Rev. D 78 (2008) 065007, arXiv:0804.4756.
[65] A. Dumitru, Y. Nara, E. Petreska, Magnetic flux loop in high-energy heavy-ion collisions, Phys. Rev. D 88 (5) (2013) 054016, arXiv:1302.2064.
[66] A. Dumitru, T. Lappi, Y. Nara, Structure of longitudinal chromomagnetic fields in high energy collisions, Phys. Lett. B 734 (2014) 7, arXiv:1401.4124.
[67] R. Baier, Yu.L. Dokshitzer, A.H. Mueller, S. Peign, D. Schiff, Radiative energy loss and $p_\perp$-broadening of high energy partons in nuclei, Nucl. Phys. B 484 (1997) 265, arXiv:hep-ph/9608322.
[68] A. Kovner, U.A. Wiedemann, Eikonal evolution and gluon radiation, Phys. Rev. D 64 (2001) 114002, arXiv:hep-ph/0106240.
[69] I.Y. Aref'eva, Holography for heavy ions collisions at LHC and NICA, arXiv:1612.08928.